

Founded 1925

Incorporated  
by Royal Charter 1961

*"To promote the advancement  
of radio, electronics and kindred  
subjects by the exchange of  
information in these branches  
of engineering."*

VOLUME 42 No. 9

SEPTEMBER 1972

# THE RADIO AND ELECTRONIC ENGINEER

The Journal of the Institution of Electronic and Radio Engineers

## Straws in the Wind

THE one essential ingredient for success in any new venture is not, one has discovered, that of being a byword of past quality like Rolls-Royce. Regrettably neither is it the possession of sufficient research potential to keep near the frontiers of knowledge: there success is precarious indeed. No, the essence of success is the ability to identify the significant trends in commerce or industry—and to act correctly on them. The broker who knows to buy when a share has touched rock-bottom and is about to rise, and can advise one to sell without qualms later when it touches its peak, has that vital ingredient for success in his world. But this is not just a matter of money. The student who chooses early a discipline which will lead to a satisfying career where there is a continuing demand for his services is as successful in his world too.

The electronics industry has had its share of ups and downs, and redundancy amongst graduates has rivalled that of the chemical industry which has more unemployed Ph.D.s than any other sector in U.K. Neither has the dock strike in August helped an industry with so large an export commitment. The computer manufacturers have suffered as much as any in the last two years with sad examples of cutback and withdrawal in research, development and production. Surely, of all times now is the most inappropriate for the I.E.R.E. and its sister institutions to mount a computer conference?

It may be that the electronics industry is no longer becalmed and the 'stock' of computing has just come through rock bottom and is on the way up. Signs of recovery in the U.S. market, the wider vistas of trade that entry into Europe will mean, and further massive government support for ICL are all straws in the wind—the kindly wind of recovery. Certainly the National Electronics Council has provoked considerable action in order to ensure the future viability of the British Computer industry. Perhaps then this is the time to take a fresh look at computing, at one's own involvement, at company involvement, at modern technology, as consultant, manufacturer or user. In the days ahead no one will be satisfied with second best, and if there is to be a continuing demand for the services of a U.K. computing industry, that challenge must be taken up now, not when overseas competition is in full spate. That is why this Institution with the co-sponsorship of the Institution of Electrical Engineers and the British Computer Society is so keen to go ahead at this time with a major computer conference.

The function of an editorial such as this is to bring important issues and events to the notice of members; it is not to enlarge on the detailed content of the conference (given on page S.141). The Conference on 'Computers—Systems and Technology' is to be held in London from 24th to 27th October. Let it suffice that even a cursory look at the preprints of the conference shows it will live up to its name and the aims of its sponsors. Large and small systems, software and hardware, and man-machine interaction are all there, with much else, treated in the up-to-date fashion that is so desperately needed now.

K. J. DEAN

## Contributors to this issue



**Mr. Richard Wyld** (Member 1972), after completing RAF service, took a course at The Polytechnic, Regent Street, London, on telecommunications engineering, and then joined Marconi's Wireless Telegraph Co., working on the development of airborne communications equipment. Five years later he went to Vickers Armstrongs (Aircraft) Ltd. at Swindon, where he designed and developed aerial systems for military aircraft.

Following regrouping in the aircraft industry he was transferred to Vickers Engineering Group, where he was engaged on the design of instrumentation and control systems applied to nuclear, industrial and medical engineering. During this period he was awarded the Society Prize of the Society of Electronic and Radio Technicians for a paper entitled 'Industrial Instrumentation and Control Systems' which was published in 1968. In January 1971 Mr. Wyld joined Marconi Space & Defence Systems, Frimley, as a Principal Project Control Officer in the Space and Instrumentation Division.



**Dr. D. W. Swift** studied at the University of Manchester, obtaining his B.Sc. in 1957, and went on to the University of Cambridge where he was awarded his doctorate in 1961 for research on electron sources for electron microscope and microprobe systems. He was employed on electron-optical systems at the N. V. Philips' research laboratories in Eindhoven, Netherlands until 1964, and then moved to the

European Space Research Organization to work on satellite development. In 1967 he joined Pilkington Perkin Elmer Ltd. as Senior Project Engineer, and completed the move from electron-optics to electro-optics which had begun in ESRO. He is now Deputy Chief Physicist at PPE. Dr. Swift is a course tutor in technology for the Open University.



**Mr. G. V. Thompson** received the B.Sc. degree in physics from the University of London in 1963, and for the next four years he was employed at the Feltham Laboratories of E.M.I. Electronics Ltd. working on infra-red transmission atmospheric studies. In 1967 he joined PPE, St. Asaph, where he is at present working on a variety of electro-optical systems including low-light-level and infra-red devices.



**Dr. W. Tempest** graduated with honours in physics from Liverpool University in 1954 and in 1957 was awarded the degree of Ph.D. from the same university. After a year in industry he joined the staff of the Electrical Engineering Department of the Royal College of Advanced Technology, Salford and in the following year returned to Liverpool University as a Lecturer in Acoustics. At Liverpool he worked in the fields

of ultrasonic propagation in gases and also became involved in a number of projects involving studies of the human hearing process. In 1963 he spent a year on leave from Liverpool to study the propagation of sound in the atmosphere at Columbia University New York. In 1966 he left Liverpool University to return to Salford University Electrical Engineering Department to establish an Audiology Group. Two years later Dr. Tempest was appointed Reader in Electrical Engineering and has continued research into a range of problems in the fields of hearing, deafness and noise.



**Mr. J. K. Moss** completed a five-year engineering apprenticeship before entering Durham University, from which he graduated in 1961 with a B.Sc. honours degree in electrical engineering. He then spent four years with Ferranti Ltd., Edinburgh as a research engineer. During this period he worked on computer and servo design for airborne radar. This was followed by two years as a systems engineer with B.A.C.,

Stevenage. Since 1967 he has been with the proposed Preston Polytechnic where he is a Senior Lecturer in the Electrical Engineering Department. Besides lecturing and associated duties he is currently researching into the development of computer models of the audiometric system in association with the Audiology Research Unit of the University of Salford



**Mr. R. J. Simpson** graduated with a B.Tech. honours degree in Electrical Engineering from Loughborough University of Technology in 1963. He was sponsored by British Aircraft Corporation and was subsequently employed as an electronic systems design engineer. Since 1965 he has been on the staff of the proposed Preston Polytechnic where he is a Senior Lecturer in Control and Com-

puter Engineering in the Electrical Engineering Department. In 1969 he was awarded an M.Sc. by Loughborough University for his research thesis on a.c. control systems. At present he is engaged in research into non-linear system identification and stabilization in association with the Electrical Engineering Department at the University of Salford and is currently completing his doctoral thesis.

# An Automatic Biochemical Analyser

R. WYLD, F.S.E.R.T., C.Eng., M.I.E.R.E.\*

## SUMMARY

A machine for the automatic analysis of human blood and other body fluids is described. Brief reference is made to the associated biochemistry. The problems of measurement of sample optical density and the control of sample temperature, are discussed, and the considerations leading to the choice of photo-cells for the analysers are considered. The analysing equipment and the means of achieving positive identification of samples are described. The requirements for controlling the machine are discussed and the application of computer-control to the machine and the logging of output data is described.

\* Formerly with Vickers Limited, Engineering Group, Swindon, Wiltshire, now with Marconi Space and Defence Systems, Frimley, Surrey.

## 1. Introduction

The growth in the volume of work in clinical laboratories has produced a shortage of technicians skilled in executing work of this nature. As a result of the increasing workload, a demand for means of accelerating and simplifying the process of biochemical analysis now exists. The design of the equipment to be described in this paper is therefore intended not only to accelerate the task of analysis, but to minimize the skill required of the operator. A bonus has been obtained in minimizing the effects of human error and thus in improving accuracy.

## 2. Basic Biochemistry of the Analyser

A superficial appreciation of the chemical processes involved is essential to understand the parameters governing the design of the equipment which is intended to carry out analyses of human blood plasma. Examples of the determinations which can be effected are albumin, glucose, cholesterol, blood urea, to name a few of the better known analyses.

The method used follows the general form already established in effecting analysis by hand. This involves the following:

- (i) Taking whole blood and separating the cells from the plasma. This is achieved by centrifuge.
- (ii) Warming the plasma to a suitable temperature.
- (iii) Adding certain chemicals in liquid form which will react in the presence of the particular blood condition under examination. This liquid is therefore known as the reagent, a different reagent or combination of reagents being required for each determination. Dilution of the plasma is also required.
- (iv) Allowing the passage of a period of time for the reaction to occur. This time will vary depending upon the particular determination being effected and the temperature at which the reaction is occurring. The period is normally a few minutes.
- (v) The effect of the foregoing is to cause a change in the colour of the sample. The depth of the colour produced provides a measure of the degree of the conditions under investigation and its assessment completes the process of analysis.

## 3. Specification

The basic requirements of the equipment were as follows:

- (i) It should be capable of carrying out up to twelve simultaneous determinations on each sample.
- (ii) It should process samples at a rate of up to 300 per hour (i.e. 3600 discrete analyses per hour).†
- (iii) Each sample and its analytical results should be positively identified.
- (iv) The design should allow the user to select the type and number of determinations.

† The latest version of the machine is capable of up to 6000 analyses per hour.

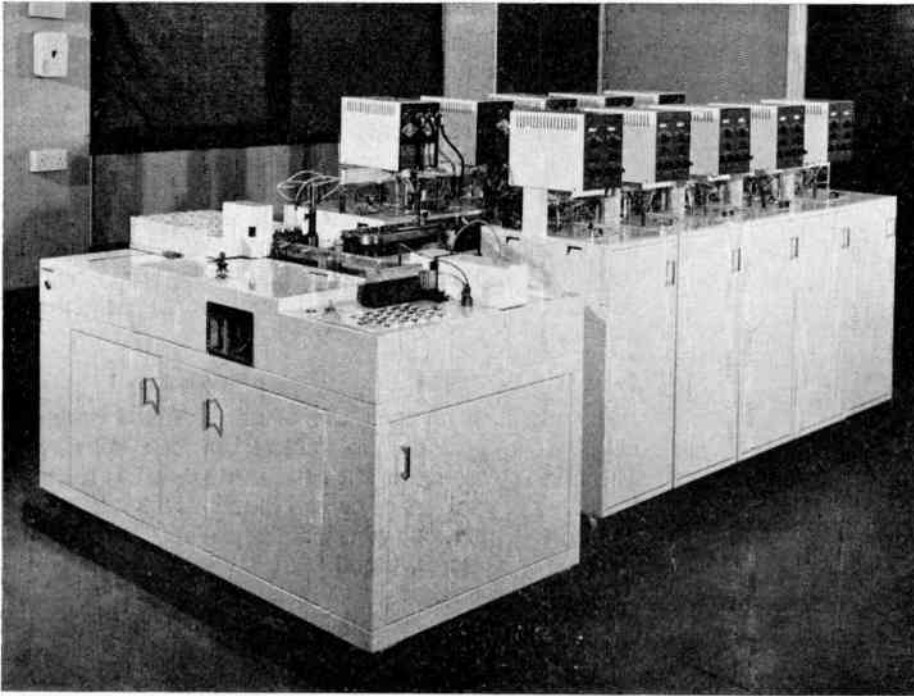


Fig. 1 (a) The Vickers automatic biochemical analyser (Multichannel 300).

From (i) and (iv) emerge the concept of separate analytical modules, each equipped with its own reagent supplies, temperature control, timing adjustment and analyser. From (ii) is inferred the need of printed results, since other forms of presentation (e.g. graphical) would be too cumbersome at such a rapid rate of operation. From (iii) the idea emerges of sealing samples in a vial which can easily be inscribed with an identifying code, for presentation to equipment which processes each sample separately and which prints the identifying code with the analytical results of each sample.

**4. Arrangement**

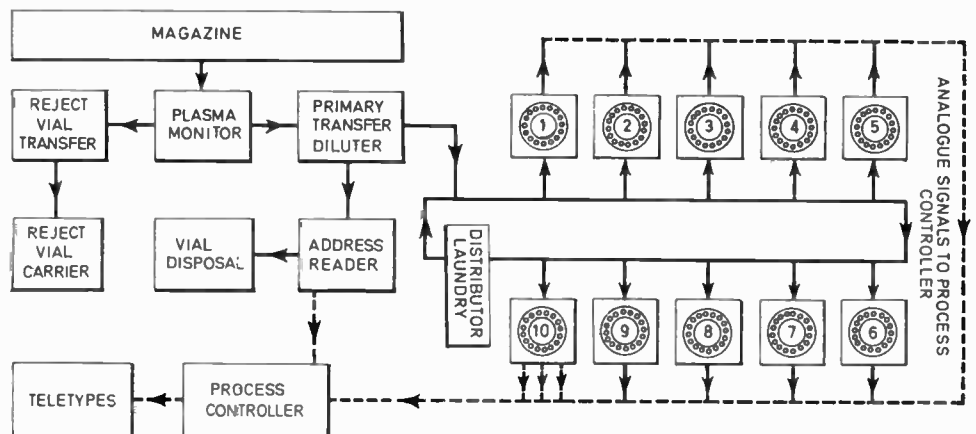
The foregoing considerations led to the arrangement shown in Fig. 1. The vials containing whole blood are coded, centrifuged, and then loaded into carriers each holding 40 vials. The magazine on the control console will accept up to eight such carriers. The vials are ejected from the carriers by spring pressure, the action being controlled electro-mechanically; they then pass to the plasma monitor which determines whether the contents of

vials are suitable for processing. The tops of accepted vials are pierced and they are then conveyed to the primary transfer diluter which extracts the plasma from the vial, dilutes it and discharges it into a cup on the distributor.

The movements of the vials take place in a series of steps: each step occurring at 12 second intervals. When the distributor cup containing the sample moves onwards one step to reaction station No. 1 the coded vial which originally contained the sample moves forward one step on the control console conveyor. This synchronism of movement between the sample and its vial is maintained throughout the process, thereby ensuring correct identification of results.

At reaction station No. 1 two quanta of the sample are withdrawn from the distributor cup, are further diluted and discharged into two pockets in a heated turntable (the reaction rotor). This advances one step every 12 seconds and requires 60 steps to complete one revolution, which thus occupies 12 minutes.

Fig. 1. (b) Arrangement of the analyser.



During this period the samples are raised to a suitable temperature, reagent and diluent in the correct quantities are added and the correct period of time for the reaction to occur elapses. The reacted sample is then presented to a colorimeter for analysis by measuring its optical density, the colorimeter output being in the form of a voltage proportional to the optical density of the sample. The reaction rotor pocket which contained the sample is washed and dried in readiness to receive the next sample.

A similar process occurs at reaction stations 2 to 10, except that each being supplied with different reagents will produce a different reaction.

The colorimeter output is converted to digital code by the process controller and, associated with the name of the analysis and the identity of the sample, is presented in printed form by a line printer. The whole process is controlled and monitored for possible faults by the process controller.

## 5. Plasma Monitor

The sample is contained in the sample vial (see Sect. 8.2) on presentation to the plasma monitor. In order that samples shall be suitable for analysis, the following conditions must be satisfied:

- (i) Sufficient quantity of sample must be present in the vial.
- (ii) The sample must have been centrifuged to separate the blood cells from the plasma.
- (iii) The turbidity of the sample must not exceed a given amount.

It is the purpose of the plasma monitor to establish that these conditions are satisfied and this is achieved by measuring the optical density of the sample under certain pre-determined conditions. The instrument is, in effect, a specialized form of colorimeter, (the principles of colorimetry are summarized in Section 6), which produces an output in one of two states, accept or reject. Failure to satisfy any one of the above conditions rejects the sample.

As blood plasma absorbs radiation between wave lengths of about 1000 nm and 2000 nm, condition (i) presents no great difficulty. The red cells, which will be packed at the bottom of the sample vial after centrifuging, are virtually opaque to incident light and condition (ii) can therefore easily be determined. Condition (iii) can be established by measuring the optical density at a wave-length of 610 nm.

The instrument consists of a light source in the form of a single tungsten filament lamp. Light falls upon one side of the sample vial via optical filters of the appropriate wavelength of peak transmission. Two photocells are situated on the other side of the vial, the uppermost detecting condition (i). The bottom photocell checks both conditions (ii) and (iii).

Silicon photovoltaic diodes type SPD 550 are used for the upper and lower level channels as shown in the simplified circuit diagram of Fig. 2. In both cases the photodiode provides the input to a general-purpose, thick-film, hybrid operational amplifier, having a differential input.

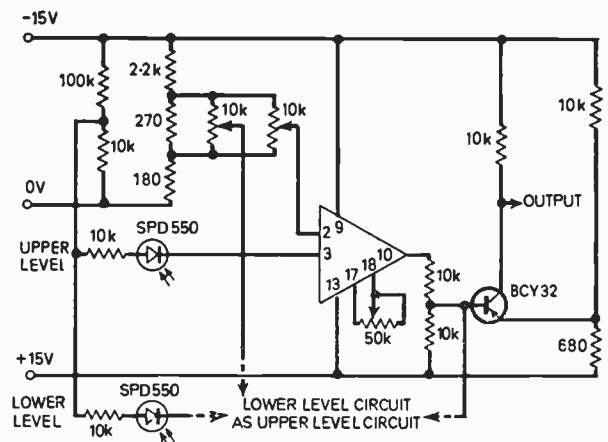


Fig. 2. Simplified circuit diagram of plasma monitor.

The amplifier has a typical open-loop voltage gain of 87 dB. The input voltage offset drift is  $\pm 20 \mu\text{V}/\text{degC}$  and the common-mode rejection ratio is 70 dB.

In the event of any one channel being activated the output transistor is switched on, producing a rejection signal. This is transmitted to the process controller for appropriate action to be taken.

## 6. Colorimeters

The purpose of the colorimeter is to measure the optical density (which is the inverse of transmission) of the sample by producing an output voltage proportional to optical density. When light is transmitted through a coloured solution some absorption occurs, the degree of absorption being governed by the Beer-Lambert Laws.†

The colour developed by the sample varies depending upon the particular reaction which the reaction console has been set to produce. The light source produces light over the spectrum 300 to 1000 nm and it becomes necessary to restrict the wavelength of the light generated to that part of the spectrum which will result in maximum absorption by the sample. For this reason an optical filter having peak transmission at the appropriate wavelength is introduced into the light beam.

Unavoidable variations in the intensity of the light source will result in error. A dual arrangement has therefore been adopted, consisting of two cuvettes and two photocells illuminated by a single light source. However, the sample is introduced into one beam only and the second photocell can therefore be used as a reference. Photo-conductive cells form two arms of a bridge arrangement; the presence of a sample in one light beam results in a rise in the resistance of that photocell. This unbalances the bridge which feeds a d.c. operational amplifier to provide the desired output. Stabilized power supplies for the bridge and the amplifier form part of the colorimeter.

† Beer's Law states that the intensity of a ray of light is inversely proportional to the thickness of absorbing material through which it has passed.

Lambert's Law states that the illumination of a surface on which light falls normally from a point source is inversely proportional to the square of the distance of the surface from the source.

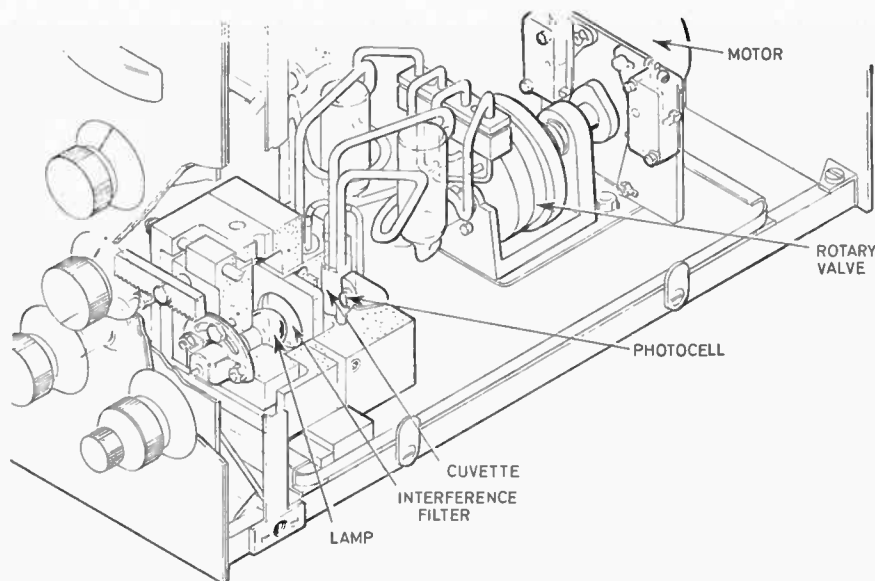


Fig. 3. Colorimeter layout, with cuvette housing cut away to reveal lamp, interference filter, cuvette, and photocell.

The sample is introduced into the colorimeter cuvette by a single vacuum pump which supplies the entire machine. Each colorimeter is fitted with a motor-driven rotary valve, the ports of which open and close at the appropriate times to fill and empty the cuvette.

The colorimeter is fitted with several controls and a meter on its front panel for initial setting up, but in normal operation is entirely automatic.

### 6.1 Layout

The colorimeters are mounted above the reaction rotors. The maximum length of the plastic tubing through which the sample is drawn on its way from the rotor to the colorimeter cuvette is critical, because traces of sample left in the tube can contaminate the next sample. It is therefore necessary to mount the cuvettes and hence the lamp and photocells in the bottom of the colorimeter and it is convenient to situate the rotary valve near them.

To minimize the possibility of electronic components being damaged by corrosive liquids should tubing become detached, they are mounted in the upper part of the chassis. A printed circuit board carries the bridge components and the operational amplifier and its associated components. The power unit is built on a sub-chassis in the upper part of the colorimeter.

In the interest of economy it is important that satisfactory performance is obtainable from a low wattage filament lamp serving as the light source and that the use of optical lenses is avoided. This means that the spacing of the photo-cells from the lamp must be as small as possible. This is particularly important in the case of reactions whose optical density must be measured at wavelengths in the blue part of the light spectrum, where filament lamps generate little output. The cuvettes, photo-cells and lamp are therefore arranged as shown in Fig. 3. The cuvettes are fitted in a light alloy casting, light from the lamp shining through two tunnels and passing through the cuvettes to reach the photocells. Optical filters can be inserted from beneath the casting.

For reasons explained in Section 6.3 the lamp is mounted on a carriage which can be moved horizontally by a knob (mounted on the front panel) and a worm drive. As the photocells are temperature sensitive they must not be allowed to touch the cuvettes containing the warm sample and heat conducted from the lamp enclosure is minimized by thermal insulation.

### 6.2 Choice of Photocells

The performance of the colorimeter is determined largely by the characteristics of the photocells. Photo-conductive bulk effect cells were chosen in preference to other types of light sensitive cell due to their high sensitivity, low cost and freedom from expensive power supply requirements. A relatively simple and inexpensive colorimeter has resulted. Photo-conductive cells are made from cadmium sulphide or cadmium selenide, the whole layer of light-sensitive material typically falling in resistance logarithmically from about 100 k $\Omega$  to a few hundred ohms as the light level increases from 1 to 1000 lux.

The considerations governing the selection of the most suitable bulk effect photo-conductive cell from amongst the considerable range available, were as follows:

- (i) **Linearity of response:** A linear response in respect of the output voltage of the colorimeter versus the optical density of the sample is required. Photo-conductive cells do not satisfy this requirement and the means of obtaining a linear response are covered in Section 6.3.
- (ii) **Spectral response:** The colorimeter is required to function over the range of wavelength 400 to 640 nm using a low wattage filament lamp as light source. The peak response of most cadmium sulphide photo-conductive cells occurs at about 550 nm and at 400 nm is only 10 to 20%. The peak response of cadmium selenide cells occurs at rather longer wavelengths and consequently they are even less sensitive at 400 nm.

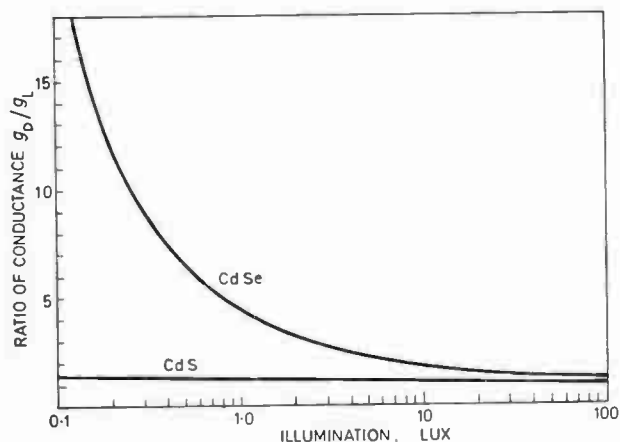


Fig. 4. Variation of conductance with light history of typical photo-conductive cells.

- (iii) Temperature coefficient: Photo-conductive cells are highly sensitive to temperature changes, CdSe cells having a greater temperature coefficient. In both CdS and CdSe cells the coefficient varies as the inverse of light level and it is therefore desirable to operate them at a high level of light intensity if possible.
- (iv) Memory effect: Photo-conductive cells exhibit this phenomenon, which is defined in Table 1, to a marked degree. It results in the conductance of a cell at a given value of light intensity, depending also upon the amount and duration of the cell's earlier exposure to light. This effect, also known as light history effect, has been dealt with fully elsewhere.<sup>2,3</sup> It is more marked in CdSe than CdS cells (Fig. 4), and presents a very real problem in using photo-conductive cells to carry out accurate measurement of light intensity.
- (v) Rate of response: CdSe cells respond to changes of light level more rapidly than CdS cells. In the cases of both cells the response is much slower at low levels of light intensity and in an automatic system where samples are presented for measurement for only a few seconds, this presents a difficulty.
- (vi) Size: The volume of the reacted sample in the cuvette amounts to less than one millilitre. The area of the light-sensitive part of the photocells must be dimensionally compatible with this.

It will be clear from the foregoing that the choice of a photocell will be a compromise. Many photo-conductive cells are intended simply for use as sensors, not for measurement purposes, and these are quite unsuitable. The specification of a suitable cell is given in Table 1.

A higher sensitivity is desirable at 400 nm but is unattainable with this type of photo-conductive cell.

The characteristics of CdS and CdSe photo-conductors and the means by which their characteristics may be modified have been dealt with by others.<sup>2</sup>

Table 1

Nominal resistance at 20 lux	10 kΩ
Nominal dark resistance	greater than 500 kΩ
Temperature response over the range 0°C to 50°C (throughout range of illumination of 1 to 10 lux)	less than 8% conductance change
Memory, defined as the ratio of conductance at 1 lux after an infinite dark history ( $g_D$ ) to conductance at 1 lux after infinite exposure at 300 lux ( $g_L$ ), ( $g_D/g_L$ )	less than 1.15
Rate of response, defined as the time to reach a factor of $[1 - (1/e)]$ of final reading, after 5 seconds dark adaptation, on exposure to a change of illumination from dark to the value stated,	
rise-time on exposure to illumination of 1 lux	less than 0.12 s
rise-time on exposure to illumination of 10 lux	less than 0.03 s
decay-time on extinguishing illumination of 1 lux	less than 0.02 s
decay-time on extinguishing illumination of 10 lux	less than 0.004 s
Spectral response,	
wavelength corresponding to peak sensitivity	between 400 and 600 nm
response at 400 nm	greater than 20% of peak sensitivity
response at 600 nm	greater than 50% of peak sensitivity

† In practice a period of 24 hours is sufficient.

### 6.3 Circuit Description

The logarithmic law of the photocells is converted to a substantially linear one by operating the cells in a bridge circuit (Fig. 5(a)) in which two arms each consist of a photocell in series with a fixed resistor. The resistance of the reference photocell does not change. If the resis-

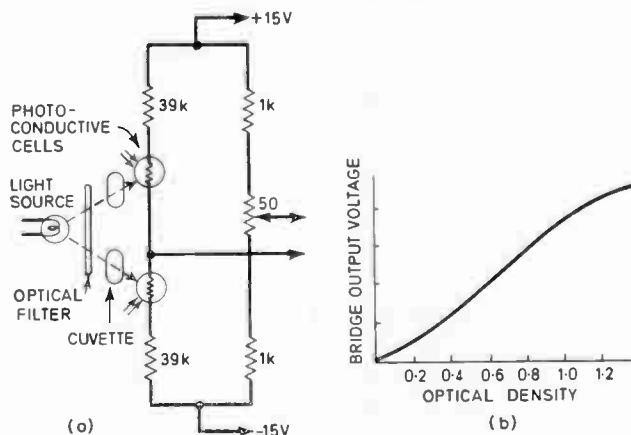


Fig. 5

- (a) Colorimeter bridge circuit.
- (b) Bridge output versus sample optical density.

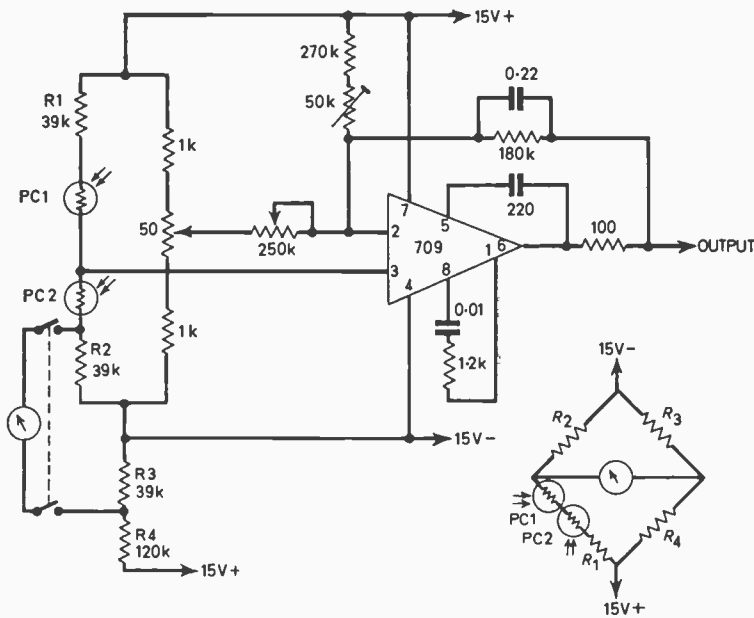


Fig. 6. Colorimeter simplified circuit diagram, with bridge balancing arrangement shown inset.

tance of the sample photocell rose by linear increments the potential at the bridge output would rise in an arithmetic progression of the terms 1/10, 2/12, 3/14, 4/16 5/18, etc.

However, as the law of the photocell is logarithmic with respect to linear increments of illumination, the effect is to produce a bridge output with respect to sample optical density of the form shown in Fig. 5(b). The departure from a linear characteristic over the range of optical density 0.1 to 1.0 is less than 1% of full scale.

The input/output characteristic of the instrument can only be correctly controlled as described above if the resistance of both cells under standard conditions, i.e. a sample optical density of zero, is known and, in the interest of simplicity, is the same.

The latter can be achieved by using cells in matched pairs. The former would present no difficulty if the transmission characteristics of the optical filters, regardless of wavelength, were the same and the amount of light generated throughout the required spectrum was constant. This problem is solved by adjusting the brilliance of the lamp to balance the resistance of the sample cell against a reference resistor on initially setting the instrument. This must, of course, be done after the filter is fitted and in the presence of a sample having an optical density of zero.

Although the photo-cells are matched and close tolerance resistors are used in the bridge, the instrument must be set to zero before adjusting the lamp brilliance as described above, the main source of error being photocell variations. This could be done by adjusting the bridge output tapping but this has the disadvantage that although the bridge is balanced, the photocells are unequal. Zero setting is therefore achieved by adjusting the position of the lamp laterally with respect to the photocells. As the light reaches the photocells via the tunnels in the cuvette block (Sect. 6.1), this has the effect of varying the illumination of each cell relative to the other and a sharply defined zero setting is obtained which ensures that the

resistance of the two photocells at the wavelength in use is the same.

The bridge drives a type 709 integrated circuit operational amplifier whose input impedance exceeds 10 MΩ, thus avoiding loading the bridge. A potentiometer in the input circuit controls the gain which is limited to 10 dB. A simplified circuit diagram is given in Fig. 6.

#### 6.4 Rotary Valve

The sample is transferred to the colorimeter by means of a probe which descends into the pocket of the reaction rotor containing the reacted sample. The sample is withdrawn under suction and is passed into the colorimeter cuvette when a port in a rotary valve is opened. When the cuvette has had sufficient time to be filled the port is closed and, after a short delay to allow turbulence in the fluid to subside, the colorimeter output is read into the computer. A second port in the valve is then opened to empty the cuvette.

The valve consists of a stationary disk with a hole through the centre to which the suction pump is connected (see Fig. 7). The filling and emptying ports are situated on appropriate radii near the edge of the same disk. A second disk, having a radial slot, rotates against the fixed disk, thus connecting and disconnecting the suction to and from the filling and emptying ports. The rotating disk is driven by a small synchronous geared motor at a speed of 6 rev/min.

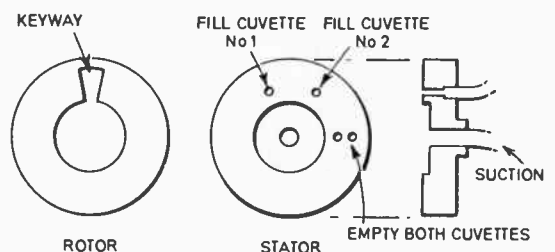


Fig. 7. Colorimeter rotary valve.

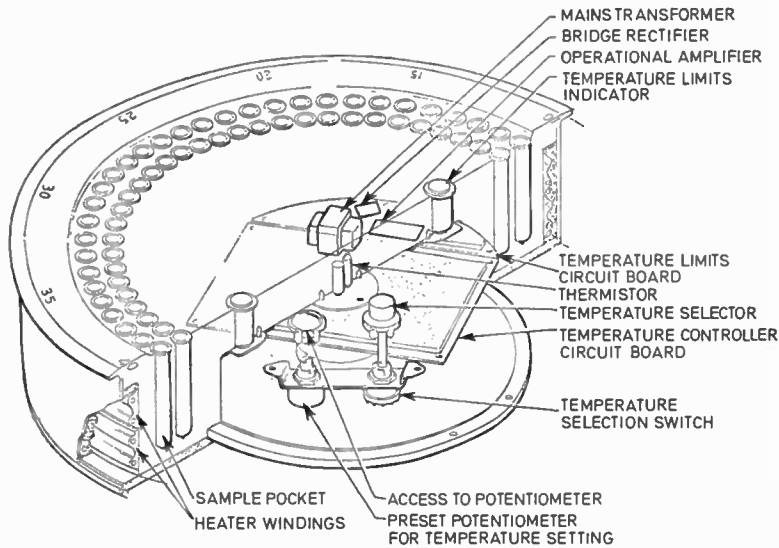


Fig. 8. Reaction rotor.

The valve must be leak proof, since minute leakage can result in movement of the sample in the cuvette, giving rise to inaccurate analysis. An adequate life of the faces of the disks before leakage occurs is obviously necessary and the materials used in the construction of the valve must resist attack by the corrosive liquids used for some reactions.

Initially the fixed disk was made in stainless steel and carbon was used for the rotating disk. This was unsatisfactory due to galvanic action in the presence of some solutions, notably chlorides. PTFE was next considered but dismissed due to its dimensional instability. Fibre-glass-loaded PTFE was tried but a leak-tight valve could not be guaranteed due to surface creep. A usable valve has been evolved by fitting a hard carbon insert into the face of the fixed disk and running a rotating disk of a different grade of carbon against it. Careful attention to surface flatness is essential.

## 7. Temperature Control of Reaction Rotors

### 7.1 The Reaction Rotor

The reaction rotor (Fig. 8) is required to heat a maximum of 120 separate reacted and diluted samples to within  $\pm 1$  degC of a predetermined temperature and maintain the samples at that temperature for a predetermined period of time. It would be prohibitively expensive to control the temperature of each sample individually and it was desired to avoid the inconvenience of the traditional method of circulating temperature controlled hot water round each sample container. The solution which was evolved consists of a heated metal turntable of large mass which holds 120 sample containers. The mass and thermal conductivity of the rotor are such that whilst the temperature at the centre of the rotor is maintained constant within  $\pm 0.25$  degC, the temperature of any sample after rising to within 1 degC of the pre-set temperature will remain within the required limits in spite of the cooling effect of other cold samples which are being discharged into the rotor. Reference to Fig. 9 will illustrate the cyclic nature of the cooling effect. Satisfactory performance depends upon careful choice of the

thermal characteristics of the rotor and upon the accuracy of the temperature controller.

Variations of temperature at the centre of the rotor are detected by a heated bead-type negative temperature coefficient thermistor. The metal-housed type of thermistor was chosen for ease of fitting in the metal rotor, the greater response time being unimportant in a loosely-coupled control system of large time-constant. The rotor is heated by a 300 W electric element wrapped round the periphery of the rotor (see Fig. 8), the input power being regulated by the controller described in Section 7.2. Proportional control is essential to meet the accuracy required. This results in the output of the controller being equal to the quantity  $(-K\theta)$ , where  $K$  is a constant and  $\theta$  is the deviation of actual temperature from required temperature. However, it is not the purpose of this paper to deal with the principles of automatic temperature control which have been discussed elsewhere.<sup>4,5</sup>

Figure 9 shows the variation of the temperature of the liquid in one pocket of a rotor during one complete cycle of the rotor.

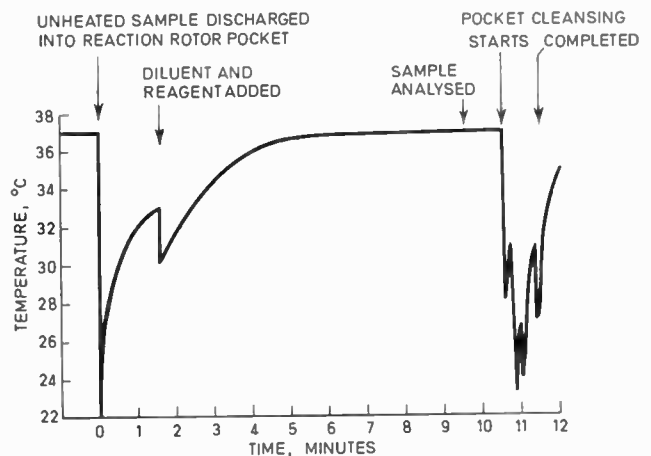


Fig. 9. Temperature cycle of reaction rotor sample pocket.

An eight-position switch on the rotor enables the user to select controlled temperatures of 20°C, 25°C, 30°C, 35°C, 37°C (blood temperature) 40°C, 45°C or 50°C.

7.2 The Temperature Controller

This is built on a circuit board mounted inside the rotor and utilizes discrete semiconductor devices to control a bidirectional thyristor (triac) which regulates the power supplied to the load. The load current is switched on and off in pulses, the on/off ratio determining the mean power dissipated in the load. The circuit shown in Fig. 10 functions in the following manner.

The output of the full-wave rectifier D3 and D4 is clipped at 18 V by the Zener diode D5. The network consisting of R2, C1 and D6 constitutes a pulse generating system, producing pulses at the zero voltage crossover point of the mains waveform. These pulses are applied to the base of a transistor TR1 acting as an emitter follower. Zener diode D7 ensures the output amplitude of the emitter follower is unaffected by variations of the mains supply.

The potential divider chain R12 to R19 enables the user to select control at the temperatures listed in Section 7.1, the highest temperature corresponding to minimum circuit resistance. Pre-set variable resistance RV2 is for use in initial setting to compensate for variations of resistance of the thermistors which have a tolerance of ±5%.

When the thermistor is cold, and its resistance is therefore high, the voltage at the anode of the silicon unidirectional switch D8 is high enough to produce conduction (it conducts when 8 V is exceeded). The RC network consisting of C3, R7, C4 and R8 starts to charge, but the charge reaches only 4 V before the end of each pulse. The capacitors then start to discharge. The combination C4 and R8 raise the base bias of transistor TR2 so that it conducts, thus enabling a train of pulses, synchronized to the mains crossover and modified to the shape of the CR envelope, to appear at the base of transistor TR3.

The output of TR3 drives the pulse transformer T2 which provides gating pulses for the bi-directional thyristor. Ringing of the transformer is controlled by diode D10. The triac is fired at the zero voltage point of the mains waveform and power is supplied to the load. As the set temperature is approached the power supplied to the load depends upon the instantaneous value of the thermistor resistance.

8. Control of the Machine

8.1 Electro-mechanical Components

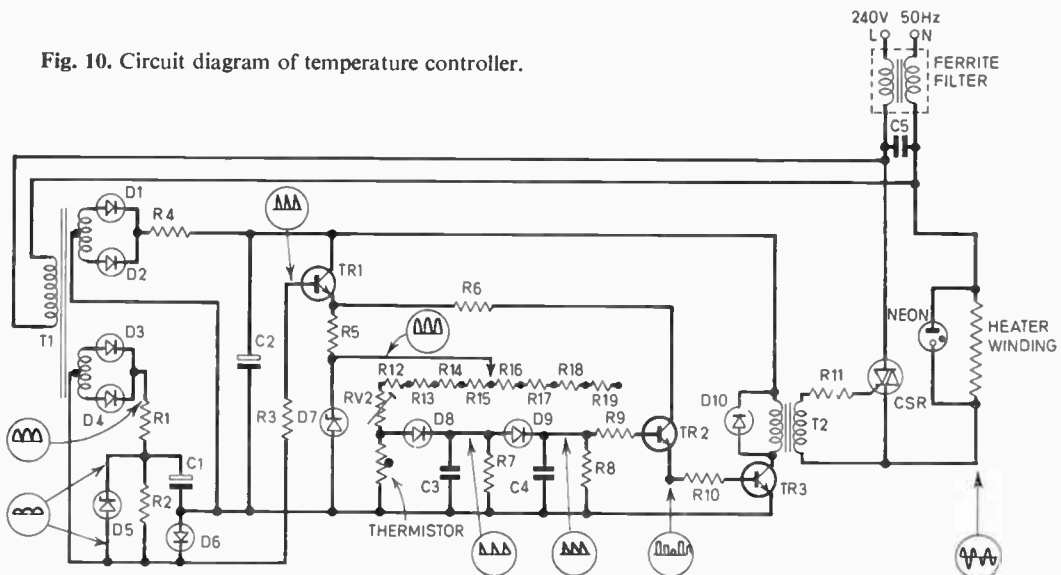
The means of achieving the actions described in Section 4 will now be considered.

Ejection of vials from the magazine (see Fig. 1(b)) under spring pressure is controlled by a solenoid. As each vial carrier is emptied the process controller is signalled accordingly, resulting in the magazine platform being allowed to move onward to align the next full carrier with the vial exit channel. When the last vial carrier comes into use, the information is relayed to the process controller by a microswitch.

The plasma monitor indicates whether the contents of vials are acceptable and the process controller energizes the appropriate solenoid to pierce the top seals of accepted vials. By energizing suitable solenoids the vials are then transferred either to the accepted or the rejected sides of a conveyor, which carries accepted vials to the primary transfer dilutor. Meanwhile, rejected vials are conveyed to a position opposite the entry to the rejected vial carrier, into which they are transferred by solenoid action at the appropriate instant.

After an accepted sample has been transferred to a distributor cup the synchronous motion of the sample in the cup and the coded vial which originally contained it, is assured by driving both distributor and vial conveyor by the same motor. A 6 rev/min geared induction motor developing a torque of 3.45 kg m (300 lb in) is used for the purpose. The motor rotates continuously and the drive is connected to the load via an electromagnetic clutch operated by the process controller.

Fig. 10. Circuit diagram of temperature controller.



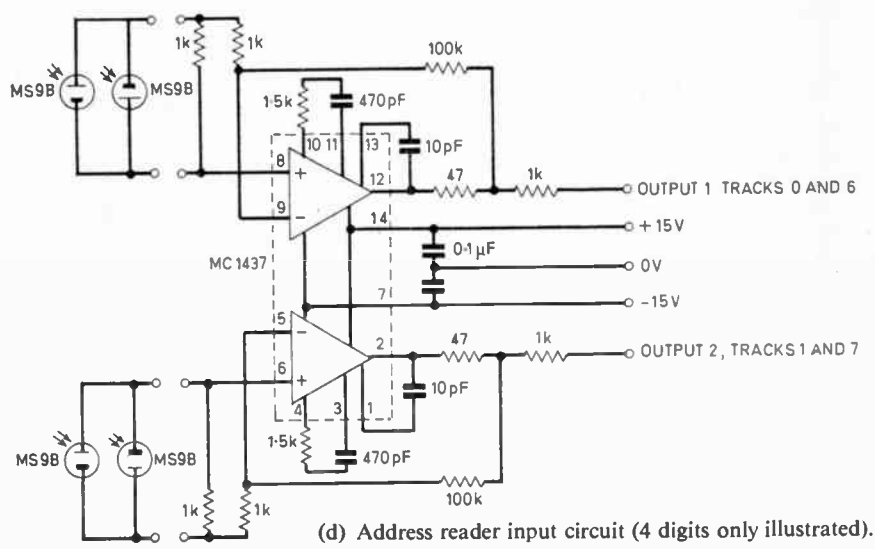
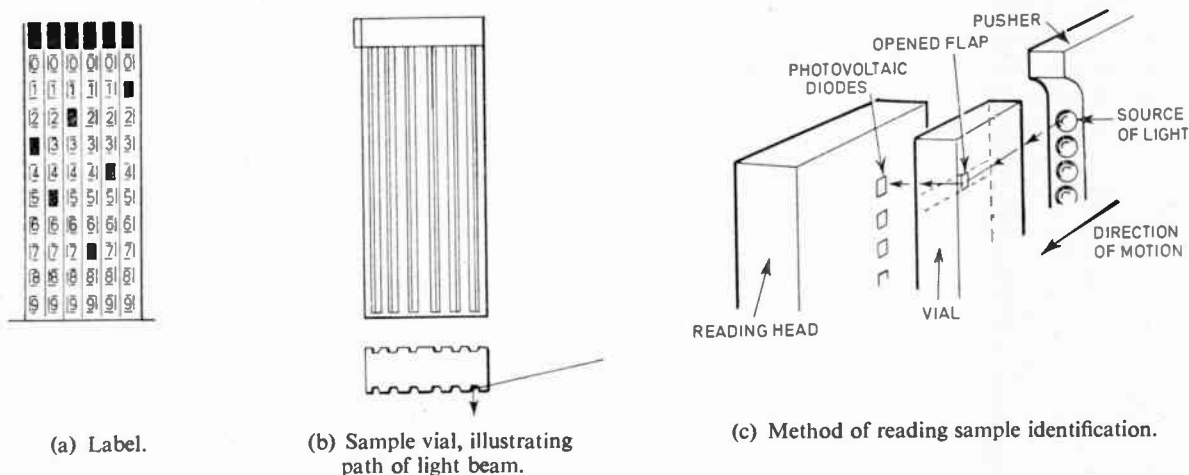


Fig. 11. Sample identification.

Failure of the mechanism to rotate as commanded is relayed to the process controller by a microswitch.

The drive for each reaction console rotor, sample probe, reagent pump and diluent pump is derived from a similar motor of 0.7 kg m (60 lb in) torque situated in each reaction console and controlled in the same fashion. Loss of synchronism by any reaction console is detected by the process controller by monitoring the action of a micro-switch operated by the mechanism of each console.

Most of the mechanisms have been designed to be operated by 70 V d.c. solenoids requiring less than 40 W of power in order to conform with the limitations of the process controller interface modules. The condition of vacuum, air and water supplies and the level of waste liquid is relayed to the process controller by pressure and level switches as appropriate.

8.2 Sample Identification

Samples are identified by means of a code impressed upon the vials which contain them. The two larger sides

of the vials carry an aluminium foil label, each side divided into six vertical columns and each column bearing the digits 0 to 9 as shown in Fig. 11(a). The larger sides of the vials have six vertical grooves (see Fig. 11(b)); when any digit on the label is pressed with suitable instrument a small flap of foil is forced into the groove behind it and lies against the inclined surface. If a beam of light illuminates the edge of the vial, some light will be transmitted along the polystyrene wall of the vial as shown in Fig. 11(b) and will be reflected by the flap through the hole in the foil left by the flap and out of the vial. If the emerging light can be detected information would be available of which digits in a column had been selected.

After the sample has been withdrawn from the vial by the primary transfer diluter (Fig. 1(b)) the vial moves step by step towards the address reader, its movements being mechanically synchronized with the motion of the sample towards the reaction rotors. On reaching the address reader station the vial is transferred from the conveyor by a pusher which emits a vertical column of

light from its front face. A similar illuminator, which takes no part in propelling the vial illuminates the rear face. The vial is steered by guides between two sensor faces, each fitted with a vertical column of ten photocells, one for each digit, on each side of the vial. As the vial moves forward each of the six vertical columns of digits is presented sequentially, for reading (Fig. 11(c)).

The flap which is pressed inwards to select a digit is about 4 mm high and small photocells are therefore essential. The MS9B silicon photo-voltaic diode was selected for this reason and is shown connected in the input circuit for one digit in Fig. 11(d). This photodiode is intended for punched tape and card reading. Suitable timing circuits (not shown) to ensure that sampling of each column of digits occurs at the correct instant in time, are also necessary. The vertical column of light for illuminating the vial is generated by ten miniature wired-in lamps which are run at less than normal rating to increase their life. No focusing is provided.

### 8.3. The Process Controller

#### 8.3.1 Control and data logging

The process controller must accept the following inputs from the machine:

- (i) Identification code of samples in the form of suitably amplified signals from the address reader photo-sensors.
- (ii) The analogue output of up to 20 colorimeters which must be resolved to at least 1 part in 900.
- (iii) Numerous alarm signals associated with loss of electrical, water, air or vacuum supplies, inadequacy of samples and electrical or mechanical failures.
- (iv) Manually-operated controls.
- (v) Input from an ASR 33 teletypewriter.

The process controller must also provide the following output facilities:

- (i) Control of a line printer providing output data in the form of identity of sample and names of tests with analytical results expressed in direct concentration units.
- (ii) Control of a magnetic tape cassette for recording output data.
- (iii) Control of the mechanical functions of the machine.
- (iv) Control of all the panel indicators and of the audible alarm associated with input and output facilities.

It had originally been intended to satisfy these requirements by using proprietary solid-state logic boards in a system expressly designed to suit the machine's control criteria. A data logger would have handled the multiplexing, analogue-to-digital conversion and printing of results. However, a computer (DEC PDP8/L) became available in 1968 at a low enough price to render computer-control of the machine worthy of serious consideration.

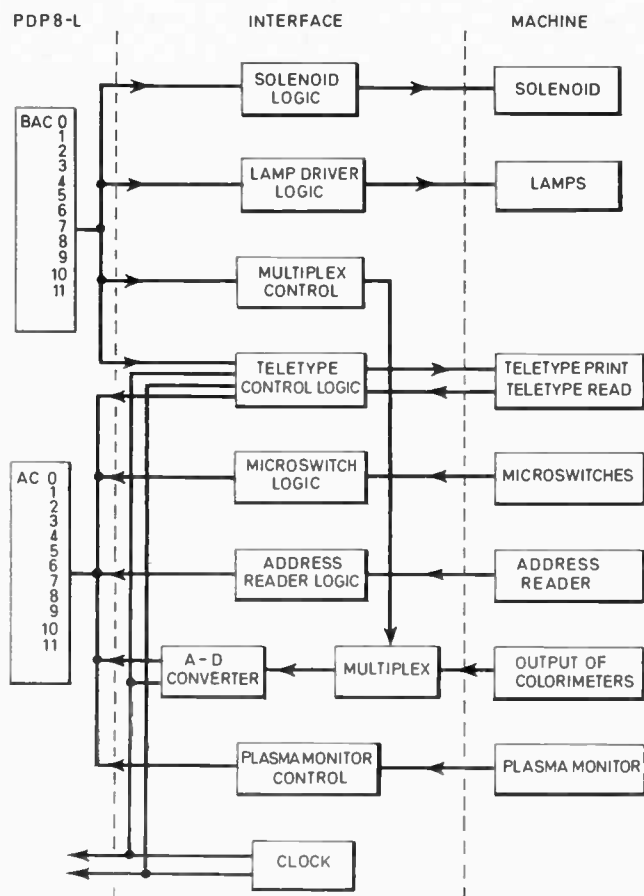


Fig. 12. Block diagram of the interface.

The use of a small computer, suitably programmed, appeared to offer the following advantages:

- (i) It would enable the introduction of automatic correction for colorimeter base line drift to be realized, by comparing results of chemical standards distributed at regular intervals amongst the samples.
- (ii) The conversion of analyser output to direct concentration units would be expedited.
- (iii) It was considered desirable, in the event of the failure of any one reaction console, that the machine would halt when those samples had been analysed. In this way 18 of the 20 analyses of each sample following the failure would be saved. Under computer control this could be a matter of suitable programming, not extra logic.

Whilst it is not suggested that the above would not be possible using a specially-designed logic system, the total requirements represent a considerable amount of logic. Furthermore, the use of a small computer confers a very desirable degree of flexibility in accommodating possible future changes by software modifications rather than hardware modification. Finally, when the machine is not in use the computer can be used off-line, for other duties.

### 8.3.2 The interface

The computer communicates with the machine and vice versa by an interface designed expressly for this purpose. D.E.C. 'M' series logic boards were largely utilized. They are high speed, transistor-transistor logic modules employing integrated circuits. A wide range of modules is available and being compatible with the D.E.C. range of computers they are an obvious choice. Figure 12 shows the interface in a block diagram form.

High current drivers are used to energize the solenoids their maximum rating being  $-70\text{ V}$ ,  $0.6\text{ A}$ . There are two drivers per module. The lamps are driven by transistor inverters producing  $-20\text{ V}$ ,  $50\text{ mA}$ . Twelve such drivers are provided per module.

The multiplexer modules contain four single-pole high-speed f.e.t. switches. Analyser analogue output signals are switched via three channels of each module whilst the fourth is used to provide a reference voltage input against which to standardize analytical channels. Four modules are therefore required to cater for the ten analyser channels. The analogue-to-digital converter is a ten-bit successive approximation unit with built-in reference supply (Fig. 13). A stable resistance-capacitance-coupled multivibrator is used to provide clock pulses.

Teletype control is achieved by a receiver module which converts a synchronous five- (or eight-) bit character teletype code to parallel form. A separate transmitter module is used to convert binary data to teletype code. Timing is derived from the clock pulses mentioned above.

The remainder of the interface logic associated with the above functions is constructed from standard modules. The interface is of course, provided with its own stabilized power supplies.

Due to the large number of inductive loads, mainly solenoids, being controlled by the interface, trouble was expected with interfering transients and this proved to be the case. All inductive loads had been diode-suppressed and care had been taken to avoid earth loops. However, a considerable amount of effort of an empirical nature in suppressing supply busbars was necessary to cure this problem.

### 9. Conclusions

This project is one which has involved many disciplines—biochemistry and mechanical, electrical and hydraulic

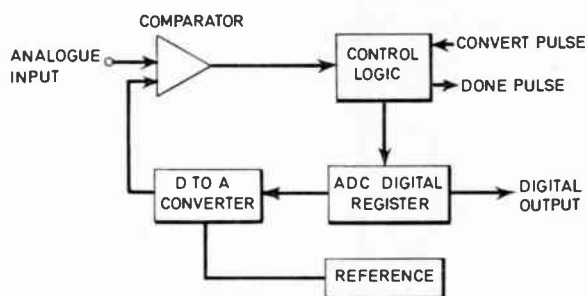


Fig. 13. Block diagram of analogue to digital converter.

engineering. The importance of team work has been manifest to those taking part.

The machine has achieved the specified performance and has led to the development of a simpler and cheaper machine which has attracted the interest of smaller laboratories. This uses one or two reaction consoles associated with a unit for feeding samples to the reaction rotors. Colorimeter output is measured by a digital voltmeter and recorded by a printer.

### 10. Acknowledgments

Development has continued since the writer was associated with this project and recent improvements have not been described.

The writer wishes to acknowledge the permission of Vickers Limited, Medical Engineering, to publish this paper.

### 11. References

- Laidler, F. R., 'Photo-electric colorimetry: Design for clinical laboratories', *Design Electronics*, 5, No. 10, pp. 24-5, July 1968.
- Bube, R. H., 'Photoconductivity of Solids', (John Wiley, New York, 1960).
- Hadley, C. P. and Fischer, E., 'Sintered cadmium sulfide photoconductive cells', *R.C.A. Review*, 20, p. 635, December, 1959.
- Coxon, W. F., 'Temperature Measurement and Control', (Heywood, London, 1960).
- Wyld, R., 'Industrial instrumentation and control systems', *Soc. Electronic Radio Technicians J.*, 2, p. 223, April-June 1968.

*Manuscript first received by the Institution on 1st December 1971 and in revised form on 7th March 1972. (Paper No. 1470/MBE 12.)*

© The Institution of Electronic and Radio Engineers, 1972

## Contributors to this issue



Dr. John Walsh received the Engineering Diploma from Memorial University of Newfoundland in 1966, the B.Eng. (Hons.) degree in Electrical Engineering from the Nova Scotia Technical College in 1968, and the Ph.D. degree in Electrical Engineering from the University of Calgary in 1971. He then spent a year as a Post-doctoral Fellow and Assistant Professor in Electrical Engineering at Sir George Williams

University, Montreal. Since June 1972 he has been at Memorial University of Newfoundland where he is currently Assistant Professor in the Faculty of Engineering and Applied Science.

Professor M. N. Srikanta Swamy is Chairman of the Electrical Engineering Department at Sir George Williams University, Montreal.

Dr. B. B. Bhattacharyya is an Associate Professor in the Electrical Engineering Department at Sir George Williams University. (Biographical notes on both these authors appeared in the July 1970 issue of the *Journal*).



Mr. H. Dunderdale spent his period of national service with the RAF, and then went to Manchester University where he graduated with a B.Sc.Tech. (Hons) Degree in 1953. He then took employment as a development engineer in the laboratory of the Computer Department of Ferranti, Moston. In 1959 he moved to the then Royal College of Advanced Technology, Salford, and he is now a lecturer in the

Department of Electrical Engineering of the University of Salford, specializing in computer technology and switching theory.



Mr. R. E. Bogner received the B.E. and M.E. degrees from the University of Adelaide in 1956 and 1959 respectively. He was a cadet engineer with the Postmaster General's Department in South Australia from 1953 to 1956 and then joined the Postmaster General's Research Laboratories in Melbourne. He worked on speech processing, acoustic techniques and subjective evaluation until 1961 when he

joined the University of Queensland as a Lecturer in Electrical Engineering. He was appointed Senior Lecturer in 1963 and was responsible for teaching and developing research in communications. His own research was mainly in signal processing and microwave measurement techniques. In 1967 Mr. Bogner joined the staff of the Imperial College, London, as a Lecturer in the Communications Section, his main research being on processing of speechlike signals.

## STANDARD FREQUENCY TRANSMISSIONS—August 1972

(Communication from the National Physical Laboratory)

August 1972	Deviation from nominal frequency in parts in $10^{10}$ (24-hour mean centred on 0300 UT)			Relative phase readings in microseconds N.P.L.—Station (Readings at 1500 UT)		August 1972	Deviation from nominal frequency in parts in $10^{10}$ (24-hour mean centred on 0300 UT)			Relative phase readings in microseconds N.P.L.—Station (Readings at 1500 UT)	
	GBR 16 kHz	MSF 60 kHz	Droitwich 200 kHz	GBR 16 kHz (Note 1)	†MSF 60 kHz		GBR 16 kHz	MSF 60 kHz	Droitwich 200 kHz	GBR 16 kHz (Note 1)	†MSF 60 kHz
1	0	+0.1	-0.1	625	612.7	17	0	0	-0.1	613	601.2
2	0	0	-0.1	625	612.7	18	0	+0.1	-0.1	613	600.0
3	+0.2	0	-0.1	623	612.8	19	0	0	0	613	600.1
4	0	+0.1	-0.1	623	612.1	20	+0.1	0	0	612	599.9
5	+0.2	+0.1	-0.1	621	610.2	21	0	+0.1	0	612	598.9
6	+0.2	+0.2	-0.1	619	608.1	22	+0.1	+0.1	0	611	598.3
7	+0.2	+0.2	-0.1	617	606.3	23	0	-0.1	0	611	599.1
8	+0.1	+0.2	-0.1	616	604.5	24	-0.1	-0.1	0	612	599.9
9	+0.1	+0.1	-0.1	615	605.1	25	-0.1	-0.1	0	613	600.4
10	0	+0.1	0	615	603.7	26	-0.1	0	0	614	600.7
11	0	0	-0.1	615	603.5	27	-0.1	-0.1	0	615	601.7
12	+0.1	+0.1	-0.1	614	602.9	28	-0.1	-0.1	0	616	602.9
13	+0.1	0	-0.1	613	602.9	29	-0.1	-0.1	0	617	605.0
14	0	0	-0.1	613	602.9	30	-0.2	-0.1	-0.1	619	—
15	0	0	-0.1	613	604.9	31	0	-0.1	0	619	—
16	0	0	0	613	601.1						

All measurements in terms of H.P. Caesium Standard No. 334, which agrees with the N.P.L. Caesium Standard to 1 part in  $10^{11}$ .

† Relative to AT Scale;  $(AT_{NPL} - \text{Station}) = +468.6$  at 1500 UT 31st December 1968.

Note 1: There is no continuity between the GBR values published for 9th April and 1st August 1972

# Seeing in the Dark

D. W. SWIFT, B.Sc., Ph.D., M.Inst.P.\*

and

G. V. THOMPSON, B.Sc.\*

*Based on a paper presented before the Northern Ireland Section of the Institution in Belfast on 16th November 1971.*

## SUMMARY

A survey of the current state-of-the-art in night vision technology is presented, including both direct vision and low light-level television systems. Possible developments in thermal imaging techniques are discussed.

## 1. Introduction

This paper presents a brief general survey of methods and devices intended to augment the performance of the eye under low illumination conditions. Since the major application of such systems is military, the latitude for description of the more advanced developments is severely limited. In recent years, however, there has been a significant increase in the civil application of night vision systems, such as for security surveillance by both police and private security organizations, and nocturnal animal behaviour studies.

The enormous range of illumination levels which occur under normal conditions is illustrated in Fig. 1. The unaided eye can cope with this range remarkably well, although not without some difficulties.<sup>1</sup> At high illumination levels the eye can resolve less than 1 arc minute, and can distinguish, for example, a 1 metre object at 1 km. Using binoculars or a telescope to provide magnification increases the range at which a given object can be distinguished in direct proportion to the magnification. As the light level is reduced below 1 lux, however, the resolution of the eye degrades partly because the eye lens aberrations increase as the iris opens more widely to collect more light, and partly because there appears to be an integration of signals from adjacent retinal detectors to boost signal level. At about  $10^{-1}$  lux it is very difficult to distinguish colour ('all cats are grey in the dark'). Between this level and  $10^{-3}$  lux, which corresponds approximately to clear starlight conditions, vision changes from photopic to scotopic. The eye is said to 'dark-adapt', which involves an increase of sensitivity, a shift in spectral sensitivity, and a further degradation of resolution: the process takes up to 30 minutes. Large high-contrast objects may be discerned down to  $10^{-4}$  lux by a young, trained observer when fully dark adapted.

## 2. Background

The performance of the unaided eye under poor illumination can be enhanced in several ways. The primary need is to collect more photons, and the most obvious way to do this is to provide auxiliary artificial illumination, which is of course the usual approach to the problem under normal conditions. It is not always appropriate however: one does not always want to advertise one's presence, not only under military conditions but also, for example, when studying animal behaviour at night: the light would change the behaviour. A World War II development was to illuminate the scene with infra-red light, obtained from a conventional incandescent lamp with a filter to remove the visible light, and to view this with the aid of an image converter tube. This contained an S1 photocathode emitting photoelectrons from light in the near infra-red, up to beyond  $1 \mu\text{m}$ . The photoelectrons were focused by an electrostatic lens onto a phosphor emitting visible light. The conversion efficiency was low so that quite powerful lamps were necessary. The disadvantages were the power requirements for these lamps and their weight and size, but above all that the system was still active: so that an enemy equipped with an image converter could readily detect the filtered lamps over distances much greater than the user of the system could detect the reflected light from his own lamps.

\* Pilkington Optical Division, St. Asaph, North Wales.

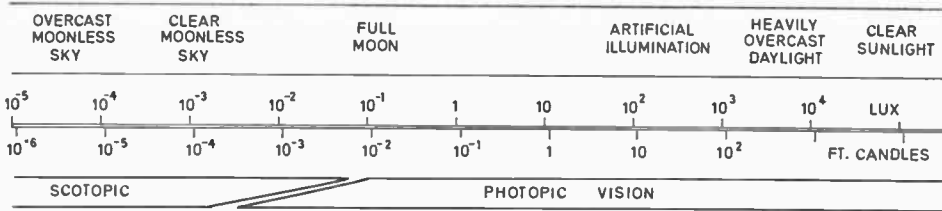


Fig. 1. Naturally occurring illumination levels.

It is therefore desirable to have a passive system; one which utilizes such natural illumination as is available. One such system, namely, the night glass, was already in use before the development of active infra-red devices. No gain in apparent brightness of the scene results from using a night glass, or binoculars: in fact the apparent brightness is constant and equal to the original scene brightness (less any losses in the optics) provided that the eye pupil is filled. This condition is satisfied if the objective diameter divided by magnification is not less than the eye pupil diameter, or approximately 7 mm when the pupil is fully open. If it is not satisfied, the apparent scene brightness will decrease. The improvement using binoculars is a result of the magnification, which improves the effective resolution of the eye: but it is a limited improvement and does not ease the problem of dark adaptation.

**3. Passive Systems**

Modern night vision systems are normally classified as either direct vision systems or low light-level television systems. The two types are not in general in competition with one another, although they may be in a given case; the direct vision system normally being preferred where portability, simplicity and reliability are required, and the television system where remote viewing, multiple displays or greater control over the display are necessary. Both types of system include an objective lens and an image tube, and the basic physics of both is the same. Whilst not going too deeply into this, it is necessary to consider it briefly in order to understand the nature of passive night vision systems.

**3.1. Background**

A major constraint on the systems is the illumination range over which they must operate, which is typically 4 orders of magnitude. A variable iris is often provided to help cope with this, but inevitably the performance in terms of resolution at the two ends of the range is limited by different constraints. At the 'high' illumination end, it is limited by the cut-off resolution  $r_1$  of the image tube. At the low end it is limited by the scarcity of photons. The arrival of the photons is random, and the quantum efficiency of the tube photocathode is less than one (typically between 1% and 10% for an image intensifier photocathode in the wavelength range of interest), so the actual limitation is the first stage photoelectron fluctuations. The low illumination resolution of a passive night vision device determined in this way is given by Richards<sup>2</sup> as:

$$r_2 = \frac{c}{4kF} \left( \frac{pstL_o}{(2-c)q} \right)^{\frac{1}{2}} \dots\dots(1)$$

- where  $c$  = contrast of scene =  $(L_o - L_s)/L_o$
- $L_o$  = higher scene luminance
- $L_s$  = lower scene luminance
- $k$  = threshold S/N factor required
- $F$  = F number of objective (= focal length/diameter)
- $p$  = objective transmission
- $s$  = integral sensitivity of photocathode
- $t$  = integration time
- $q$  = electronic charge

$r_1$  and  $r_2$  are the limiting values at the extremes of illumination, in terms of cycles per unit length at the photocathode. In general the effective resolution is approximately  $r$ , where

$$r = \left( \frac{1}{r_1^2} + \frac{1}{r_2^2} \right)^{-\frac{1}{2}} \dots\dots(2)$$

The performance of night vision systems is often characterized by the range at which a scene element of a given size can be detected, recognized or identified. These are subjective criteria which are subject to some variation of interpretation, but broadly they correspond to 1, 4 and 8 resolved cycles across the scene element respectively.<sup>2,3</sup> Figure 2 shows the way in which range depends upon illumination for a typical device. It is important to note that the range of a device is a significant piece of information only if all the appropriate conditions are stated or correctly understood. These conditions are the ambient illumination, the size, reflectivity and contrast with the surroundings of the assumed target; and the characteristics of the atmosphere, which is normally assumed to be completely transparent. It is also necessary to specify the range type—detection, recognition, or identification—being quoted.

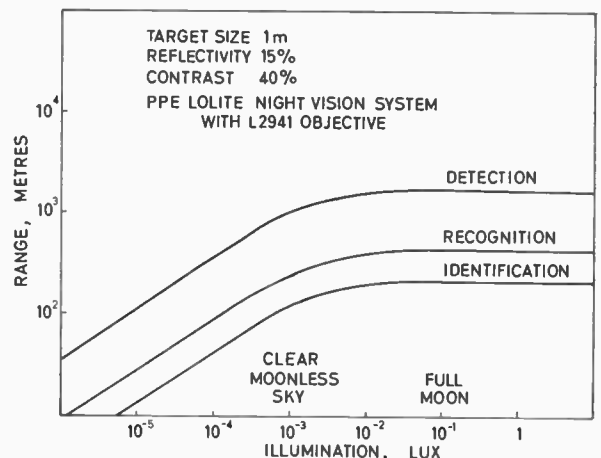


Fig. 2. The relationship between range and illumination for a typical night vision system.

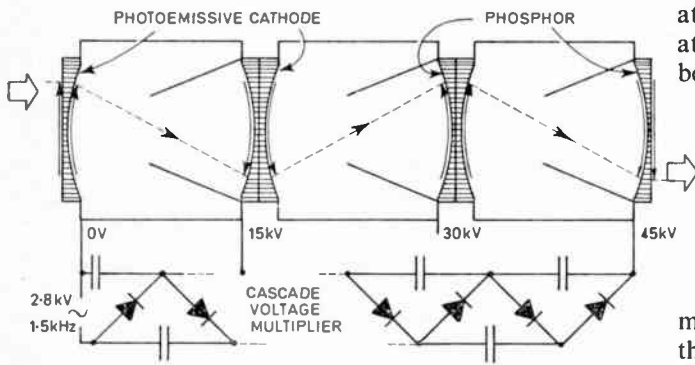


Fig. 3. Schematic diagram of a three-stage image intensifier.

at low spatial frequencies is sacrificed for an improvement at higher frequencies, up to 100 cycles per mm and beyond.

### 3.2. Objectives

The performance of a passive night vision system is very largely determined by the characteristics of the objective lens used.<sup>4-6</sup>

Range is given by

$$R = frd/n \quad \dots\dots(3)$$

where  $f$  is objective focal length,  $r$  is photocathode resolution,  $d$  is target dimension and  $n$  a factor (1, 4 or 8) dependent upon range definition.

For photon limited operation therefore, from equations (1) and (3)

$$R \propto Dc(2-c)^{-1/2} p^4 \quad \dots\dots(4)$$

where  $D$  is objective diameter.

The basic requirements for the objective are therefore a large diameter—physically to collect more photons—low losses, and a good contrast transfer at the spatial frequencies of interest which means below the cut-off resolution of the tube, in the range 0-25 cycles per mm. This latter requirement is markedly different from a good camera objective, for example, where contrast transfer

There are of course many other requirements which must be satisfied by the night vision objective. One is that it must provide the correct field of view with the selected tube format and this determines the focal length. The requirement for large diameter is therefore equivalent to a requirement for small relative aperture, or  $F$ -number. Typically, refracting night vision objectives are  $F1$  or below, and catadioptric objectives (hybrid reflecting/refracting systems) between  $F1$  and  $F1.5$ , although very large diameter or very wide angle systems will normally have larger  $F$  numbers.

### 3.3. Direct Vision Systems

A typical direct vision device consists of an objective, an image intensifier tube, and a magnifier (eyepiece). The image intensifier is a tube similar in basic construction to the image converter already mentioned, but most commonly consisting of three nominally identical stages coupled together (Fig. 3). The phosphor of the first stage is coupled to the photocathode of the second and the phosphor of the second to the photocathode of the third by means of fibre-optic face plates, the development of which has made the multi-stage tube practicable. These plates are made up of large numbers of optical glass fibres, each clad with glass of a lower refractive index, running parallel to one another from one face of the plate to the other. The individual fibres have a

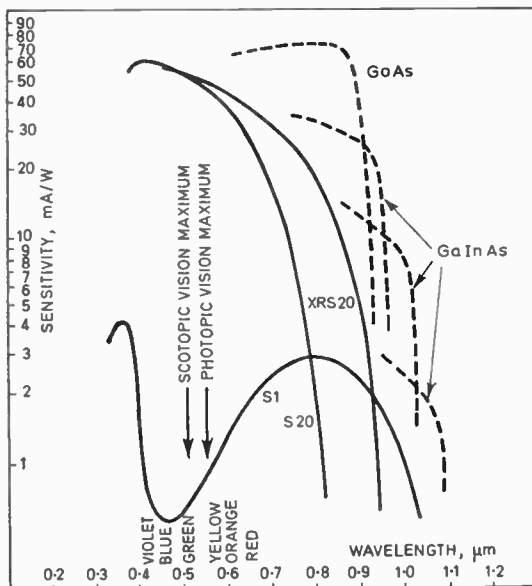


Fig. 4. Photocathode spectral sensitivities. The dotted curves are III-V reflective photomultiplier photocathodes.

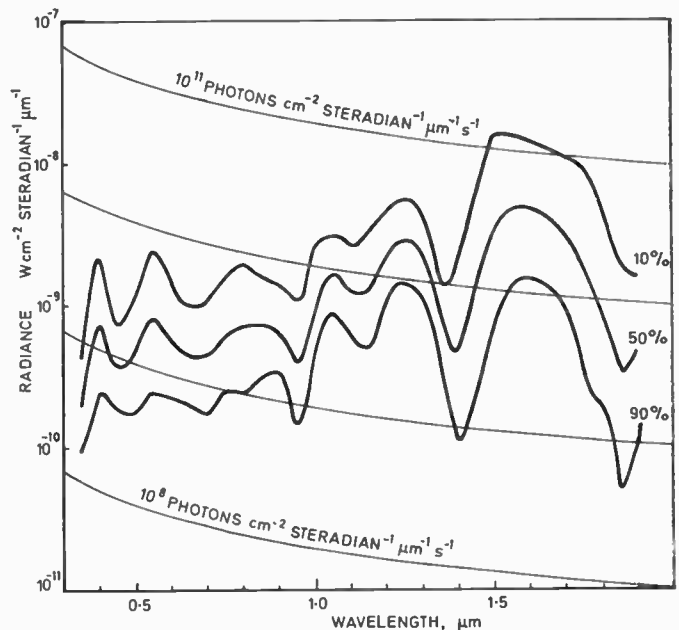


Fig. 5. Radiance of the moonless night sky (after Martin<sup>15</sup>). The three curves indicate levels exceeded for 10%, 50% and 90% of total time.



Fig. 6. PPE Lolite direct viewing system. This device has a 20° field of view and the range characteristics shown in Fig. 2.

diameter of approximately 60 μm and so allow good resolution to be maintained whilst transferring images from one face to another with very small losses. The efficient coupling is only part of the advantage however; in addition the plates are curved on the inside to match the image curvature of the electron optics, and plane on the outside to facilitate coupling and (at the front and back of the complete tube) to match the flat image planes of the light optics.

A three-stage image intensifier typically has an overall light amplification of up to 10<sup>5</sup>. The first stage is selected for low noise characteristics—second and third stages are much less critical—before assembly. The 3 × 15 kV supply is derived from a cascade voltage multiplier (Cockcroft-Walton ladder) built round the intensifier and encapsulated with it, which is driven by a small oscillator

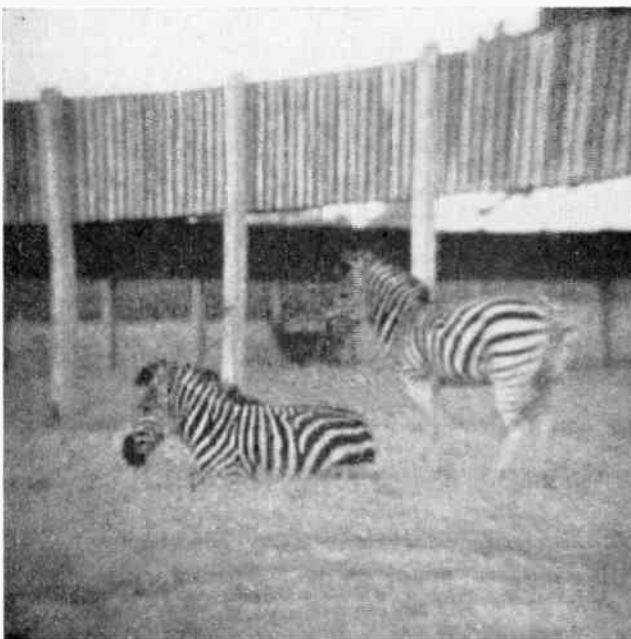


Fig. 7. Photograph taken on an overcast moonless night using the system illustrated in Fig. 6.

either also encapsulated with the tube or more commonly separate from it. The oscillator operates directly from a 6.75 V mercury battery. Overall tube magnification is in most cases nominally unity but in fact the tubes introduce severe pincushion distortion giving greater magnification at the edge than in the centre. Intensifiers are available in several sizes, notably 18, 25 and 40 mm photocathode diameter.

The photocathode sensitivity of most current tubes is S20, which extends through the visible to about 0.8 μm in the near infra-red (Fig. 4). This is an attempt to match the spectral distribution of light from the moonless night sky shown in Fig. 5.

This light is commonly referred to as starlight and the practice has been followed in this paper, but in fact the light from stars constitutes the smallest of the major three components.<sup>7</sup> The other two are the zodiacal light, i.e. sunlight scattered by interplanetary dust; and the night airglow, which is atomic and molecular emission from the upper atmosphere, principally from the hydroxyl radical OH. (The airglow is visible as a bright band above the horizon in satellite photographs of the dark side of the earth.)

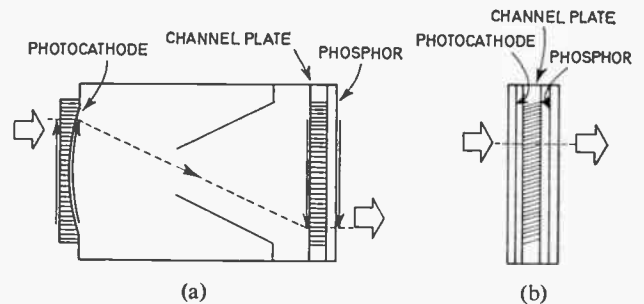


Fig. 8. (a) Single stage (inverter) channel plate image intensifier. (b) Proximity focus channel plate image intensifier.

Moonlight, which is reflected sunlight of course, is much 'bluer'; but the need for optimization is less acute under moonlight conditions because there is in any case much more light available. The point was not mentioned in Section 3.2, but the broad spectral coverage which is desirable and to some extent supplied by the S20 photocathode is a further important constraint on the objective and in the case of a refracting objective it is a severe one. The intensifier phosphor is P20, principally to provide good matching between stages.

Figure 6 shows an example of a direct vision device. This is the PPE 'Lolite' which uses a 25 mm 3-stage image intensifier and a specially designed 86 mm diameter F0.74 lens. It provides a 20° field of view, and a recognition range of 250 metres for a 40% contrast, 15% reflectivity object 1 metre in size in clear starlight. Figure 7 is a photograph taken using this device in slightly overcast starlight conditions; in this case, untypically, the principal scene element has high contrast and high reflectivity!

Since the image intensifier tube is the largest element in such a device, it is not surprising that work has been directed towards making it smaller. This has led to the

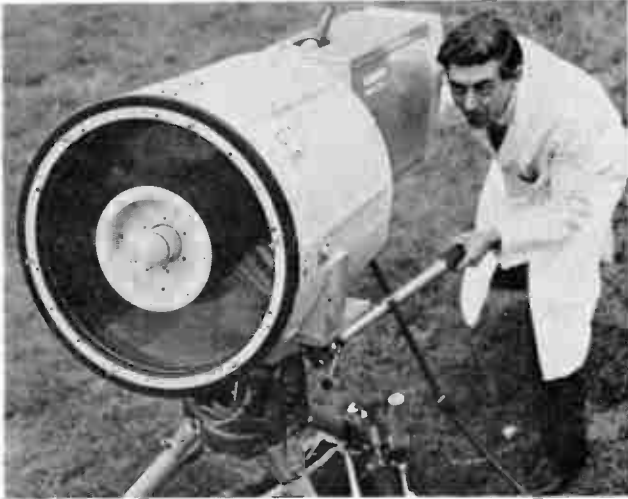


Fig. 9. Low light-level television system consisting of a PPE 508 mm diameter catadioptric objective and a Marconi camera using an isocon tube.

development of the channel plate image intensifier shown diagrammatically in Fig. 8.<sup>8,9</sup> The channel plate itself consists of many short, parallel, channel electron multipliers, each of which is a hollow glass tube with a special coating on the inside wall and a potential difference of about 1 kV between its ends. The coating has two functions: it acts as a resistor to produce an approximately linear variation of potential down the tube, and as a secondary electron emitter so that a considerable electron gain is produced as the electrons bounce along the tube under the influence of the electric field. In construction it is rather similar to the fibre-optic faceplate. The channel plate can either be used in conjunction with a conventional electron-optical imaging stage or directly using proximity focusing as shown in Fig. 8. The device, which is still under development, has recently become available on the civil market.

### 3.4. Low Light-Level Television

The optical requirements for low light-level television systems are very similar to those for direct vision devices: indeed they may be identical, since one approach to l.l.l. t.v. is to use an image intensifier stage coupled to a television camera tube. The coupling makes use of fibre optic plates once again, in a similar way to the coupling between the intensifier tube stages. Three camera tubes are of particular importance for l.l.l. t.v. work: the isocon, a derivative of the image orthicon; the s.e.c. (secondary electron conduction) vidicon, and the s.i.t. (silicon target) vidicon.<sup>10</sup>

Each of these is able to provide electron amplification within the tube itself and so may be used directly, although the image intensifier coupled arrangement provides the best performance at very low illumination levels.

The amplification in the case of the isocon is obtained by passing the return beam into an electron multiplier of conventional type, as in the image orthicon. The isocon differs from the image orthicon principally in that the return beam is composed of non-specularly reflected electrons.

In the s.e.c. vidicon, photoelectrons emitted from the photocathode are accelerated into a low density potassium chloride target, where they produce secondary electrons. The resulting conductivity changes in the target are then used to generate a signal in the vidicon mode.

The s.i.t. vidicon is somewhat similar to the s.e.c. vidicon in that photoelectrons are accelerated into a target where they produce conductivity changes. In this case, however, the target is silicon and electron-hole pairs are produced.

Figure 9 shows a l.l.l. t.v. system using a Marconi isocon camera. The objective is a 508 mm diameter catadioptric optical system and is one of the largest night vision objectives to have been built.

## 4. Development

Development is still in progress on intensifier and television camera tubes. One major direction has already been mentioned. The need for smaller size has produced the channel plate intensifier. A second area of continuing work is on the photocathodes. In recent years the sensitivity has been extended to beyond  $0.8 \mu\text{m}$  by the use of bi-alkali photocathodes, and already photo-multiplier reflexion photocathodes are available which extend beyond  $0.9 \mu\text{m}$  using the Group III-V materials. Work on transmission cathodes is in progress, particularly in the U.S.A., and no doubt image intensifiers using these materials will become available before too long. Some further development of special-purpose tubes may also occur; for example, tubes with longer integra-

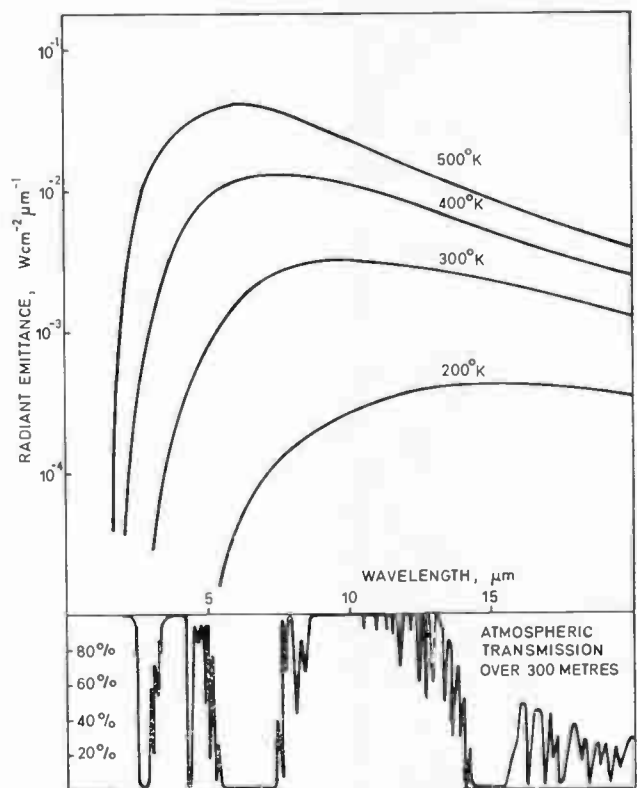


Fig. 10. Spectral distribution of energy emitted by black bodies. The lower curve shows transmission per 300 m of atmosphere and indicates the useful atmospheric windows.

tion times would appear to make sense. Range under low illumination conditions is proportional to the square root of integration time, and many applications do not require the 0.2 second response of current systems, limited by the eye. Such possibilities are severely limited by economics, however. The total market for image intensifiers is itself limited, and the market for special-purpose tubes is too small to justify extensive development.

#### 4.1. Thermal Imaging

The principal line of development, however, is in thermal imaging. Instead of attempting to detect moonlight and starlight reflected from the scene, it is possible to detect radiation emitted by the scene itself. From Fig. 10, which shows the radiation emitted by black bodies at various temperatures, it will be seen that the peak emission from objects at normal temperatures occurs at around  $10\ \mu\text{m}$ , the so-called thermal infra-red. The atmosphere absorbs most infra-red radiation, but there is a high-transmission 'window' extending from about 8 to  $14\ \mu\text{m}$ , and it is in this region that thermal imaging devices operate. The advantage is a large gain in available energy, and complete independence from the ambient illumination conditions: such a device can provide vision even in a completely dark space such as a deep cave. The disadvantages are that until recently the only suitable detectors were single element (necessitating scanning) and having either very slow response or requiring cooling; and that the resolution attainable is limited by the long wavelength to over ten times worse than the near infra-red passive systems. Existing thermal imaging systems are scanning systems, but the detector situation is currently changing as a result of the effort which has gone into this area, and one or two developments show great promise. Perhaps the most exciting is the pyroelectric detector, usually triglycine sulphate or TGS.<sup>11,12,13</sup> It is a bolometric detector but has a fast response, does not need cooling and can be used in an imaging mode. In this mode a slab of TGS is made the target of a vidicon-type camera tube, with the thermally-generated surface charge being scanned off by an electron beam in the usual way. The pyroelectric vidicon is being developed in the U.K. by the English Electric Valve Company.<sup>14</sup>

#### 5. Conclusions

An attempt has been made to present a coherent and balanced picture of the current situation in night vision. Much more could be said, but the field is too large to permit any one topic to be examined in detail in a paper

of this nature. It is a field in which much has happened in a relatively short time, and in which much is still occurring.

#### 6. Acknowledgments

The authors wish to thank the directors of Pilkington Optical Division for permission to publish this paper.

#### 7. References

1. Rose, A., 'The sensitivity performance of the human eye on an absolute scale', *J. Optical Soc. of America*, **38**, pp. 196-208, February 1948.
2. Richards, E. A., 'Fundamental limitations in the low light level performance of direct-view image intensifier systems', *Infra-red Physics*, **8**, pp. 101-15, 1968.
3. Soule, H. V., 'Electro-optical Photography at Low Illumination Levels', (John Wiley, New York, 1968).
4. Koehler, H., 'Objectives for image converters and image intensifiers', *Applied Optics*, **7**, pp. 1035-41, June 1968.
5. Richards, E. A., 'Limitations in optical imaging devices at low light levels', *Applied Optics*, **8**, pp. 1999-2005, October 1969.
6. Huxford, R. B., 'Design consideration of large aperture lens systems'. Proc. of Conference on Electro-Optics, Brighton, pp. 58-70, 1971.
7. Roach, F. E., 'The light of the night sky, astronomical, interplanetary and geophysical', *Space Science Reviews*, **3**, pp. 512-40, 1964.
8. Guest, A. J., Holmshaw, R. T. and Manley, B. W., 'Channel multiplier plates for imaging applications', *Advances in Electronics and Electron Physics*, **28A**, pp. 471-86, 1969.
9. Guest, A. J., 'Channel multiplier plates for image intensification', *Mullard Technical Communications*, No. 108, pp. 170-6, November 1970.
10. Gildea, J., 'Low light level t.v. techniques', *Applied Optics*, **9**, pp. 2230-5, October 1970.
11. Astheimer, R. W. and Schwarz, F., 'Thermal imaging using pyroelectric detectors', *Applied Optics*, **7**, pp. 1687-95, 1968.
12. Putley, E. H. and Ludlow, J. H., 'Pyroelectric detectors', Proc. Conference on Electro-Optics, Brighton, pp. 71-7, 1971.
13. Baker, G., Charlton, D. E. and Lock, P. J., 'High performance pyroelectric detectors', *The Radio and Electronic Engineer*, **42**, pp. 260-4, June 1972.
14. Holeman, B. R. and Wreathall, W. M., 'Thermal imaging camera tubes with pyroelectric targets', *J. Phys. D. (Applied Physics)*, **4**, pp. 1898-1909, December 1971.
15. Martin, M. D. and Barkess, G. P., 'The Simulation of Night sky Radiation in the SRDE Dark Tunnel'. SRDE Memorandum, No. VI/72, 1972.

Manuscript received by the Institution on 17th May 1972. (Paper No. 1471/AMMS50.)

© The Institution of Electronic and Radio Engineers, 1972

# Design of Active Distributed RC-Filters using Exponential Lines

**J. WALSH**, B.E.(Hons.), Ph.D.\*

and

**Professor M. N. S. SWAMY**,  
B.Sc.(Hons.), D.I.I.Sc., M.Sc., Ph.D.†

## SUMMARY

New active distributed RC-structures utilizing exponential RC-lines and operational amplifiers are proposed for realizing band-pass transfer functions and transfer functions having both a pair of complex poles and a pair of complex zeros. It is shown that the magnitude of the amplifier gain for a given pole  $Q$  decreases with increasing taper. In the case of the structures realizing both complex poles and zeros, it is shown that the sensitivity with respect to the gain of the pole determining amplifier is considerably lower than that of the structure previously proposed by Ghausi and Bello.

\* Formerly at Sir George Williams University, Montreal; now at the Memorial University of Newfoundland, St. John's, Newfoundland, Canada.

† Department of Electrical Engineering, Sir George Williams University, Montreal, Canada.

## 1. Introduction

The problem of designing active RC-filters utilizing distributed structures has been considered by several authors.<sup>1-5</sup> Although attention has largely focused on realizing low-pass structures some consideration has also been given to other types of filters.<sup>1,2</sup>

In this paper, new structures are proposed for realizing band-pass transfer functions and transfer functions having both a pair of complex poles and a pair of complex zeros. Detailed design procedures are described and explicit equations for the dominant critical frequency locations are given. In the case of the band-pass structure it is shown that the frequency-response very closely approximates that of a second-order band-pass transfer function. It is also shown that for the structures realizing complex poles and zeros, any of the sensitivity functions with respect to the gain of the pole determining amplifier, is considerably lower than that of a structure previously given by Ghausi and Bello.<sup>1</sup>

The use of tapering for reduction of sensitivity in the Kerwin low-pass structure is well known.<sup>3-5</sup> In this paper it is shown that tapering, in the form of an exponentially tapered RC-line (ERC), may be used effectively to control the gain of the pole-determining amplifier in the proposed structures.

## 2. Band-pass Realization

Consider the network of Fig. 1 where  $\mathcal{L}_1$  is an ERC and  $\mathcal{L}_2$  is a uniform RC-line (URC). Let the distributions of  $\mathcal{L}_1$  and  $\mathcal{L}_2$  be

$$r_1(x) = r_{01} e^{2\beta x}, \quad c_1(x) = c_{01} e^{-2\beta x} \quad (0 \leq x \leq l_1) \quad (1)$$

$$r_2(x) = r_{02}, \quad c_2(x) = c_{02} \quad (0 \leq x \leq l_2) \quad (2)$$

Then the transfer function of this network is

$$T_b(s) = T_1(s) \cdot T_2(s) \quad \dots\dots(3)$$

where

$$T_1(s) = \frac{k_1(A_1 - 1)}{A_1 - k_1} \quad \dots\dots(4)$$

$$T_2(s) = \frac{k_2}{(1 - k_2)A_2 + k_2} \quad \dots\dots(5)$$

$$A_1 = \exp(-\beta l_1) \left\{ \cosh \theta_1 + (\beta l_1) \frac{\sinh \theta_1}{\theta_1} \right\} \quad \dots\dots(6)$$

$$A_2 = \cosh \theta_2 \quad \dots\dots(7)$$

$$\theta_1 = \sqrt{(\beta l_1)^2 + s(r_{01} c_{01} l_1^2)} = \sqrt{(\beta l_1)^2 + s(RC)_1} \quad \dots\dots(8)$$

$$\theta_2 = \sqrt{s(r_{02} c_{02} l_2^2)} = \sqrt{s(RC)_2} \quad \dots\dots(9)$$

We shall use pole-zero cancellation such that equation (3) approximates a second-order band-pass transfer function of the form

$$\frac{s}{s^2 + 2\omega_n \cos(\delta)s + \omega_n^2} \quad \dots\dots(10)$$

where  $\delta$  is the angle measured from the negative real axis to the complex pole position in the  $s$ -plane.

In order to show how the network of Fig. 1 may be used to approximate equation (10) by using the pole-zero cancellation technique, let us first consider the case

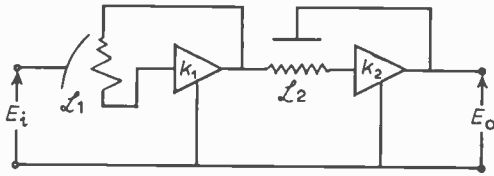


Fig. 1. Proposed band-pass structure.

where  $\mathcal{L}_1$  is also a URC (that is  $\beta = 0$ ).

The zeros of  $T_1(s)$  are now given by

$$\cosh \theta_1 - 1 = 0 \quad \dots\dots(11)$$

and, hence, are

$$s = -\frac{(2n\pi)^2}{(RC)_1}, \quad n = 0, \pm 1, \pm 2, \dots \quad \dots(12)$$

It is readily seen that one of these zeros is at the origin and all others are double zeros on the negative real axis. Since we are interested in a band-pass structure the effect of the double zeros should be eliminated.

Choose the amplifier gain  $k_2$  in Fig. 1 equal to 0.5 so that  $T_2(s)$  in equation (3) has double poles.<sup>3</sup> These poles are given by

$$\cosh \theta_2 + 1 = 0 \quad \dots\dots(13)$$

and, hence, are

$$s = -\frac{\{\pi(1+2n)\}^2}{(RC)_2}, \quad n = 0, \pm 1, \pm 2, \dots \quad \dots\dots(14)$$

Select  $(RC)_2$  such that the first pair of double poles of  $T_2(s)$  coincides with the first pair of double zeros of  $T_1(s)$  or

$$(RC)_2 = \frac{(RC)_1}{4} \quad \dots\dots(15)$$

The given pole pair of equation (10) may be realized<sup>3</sup> by the dominant poles of  $T_1(s)$ .

Figures 2(a) and (b) show the normalized frequency responses of the network of Fig. 1 ( $\mathcal{L}_1$  being a URC) and that of the band-pass function (10) for  $\delta = 89.4^\circ$  ( $Q \approx 50$ ) and  $\delta = 87.14^\circ$  ( $Q \approx 10$ ). Thus our assumption that cancellation of the first set of double zeros of  $T_1(s)$  with the first set of double poles of  $T_2(s)$  to realize equation (10) is justifiable. However the value of  $k_1$  is large (see Table 1).

It will be shown that this pole-zero cancellation technique can still be used even when  $\mathcal{L}_1$  is an ERC and that  $k_1$  can be reduced by increasing the taper  $\beta l_1$ .

When  $\mathcal{L}_1$  is an ERC, the zeros of  $T_1(s)$  are given by

$$\cosh \theta_1 + (\beta l_1) \frac{\sinh \theta_1}{\theta_1} - \exp(-\beta l_1) = 0 \quad \dots\dots(16)$$

where  $\theta_1$  is given by equation (8). Obviously there is a simple zero at the origin, but the other zeros are not easily determined since equation (16) cannot be solved in closed form for  $\theta_1$ . For design purposes it is assumed that the zeros of equation (3), apart from that at the origin, are approximately given by

$$\cosh \theta_1 - 1 = 0 \quad \dots\dots(17)$$

or

$$s = -\frac{\{(2\pi n)^2 + (\beta l_1)^2\}}{(RC)_1}, \quad n = \pm 1, \pm 2, \dots \quad (18)$$

If  $k_2$  is again chosen to be 0.5, then the poles of  $T_2(s)$  are given by equation (14). Again cancelling the first set of poles of  $T_2(s)$  with the first set of approximate zeros of  $T_1(s)$  we get

$$\frac{\pi^2}{(RC)_2} = \frac{(2\pi)^2 + (\beta l_1)^2}{(RC)_1} \quad \dots\dots(19)$$

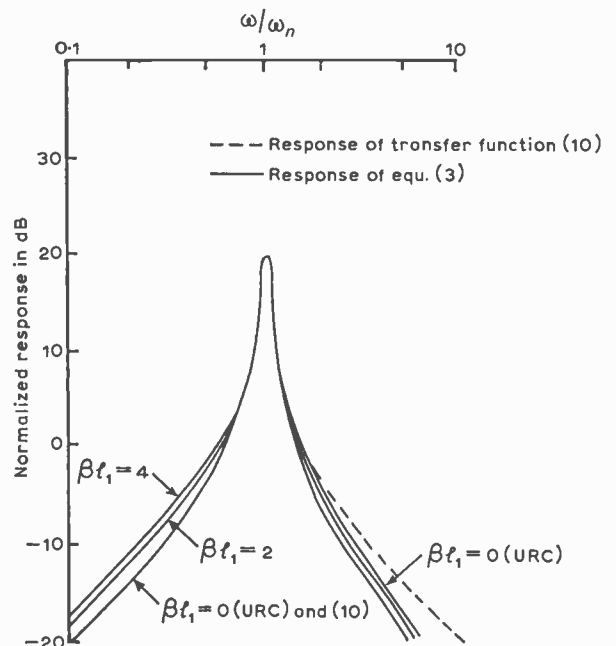
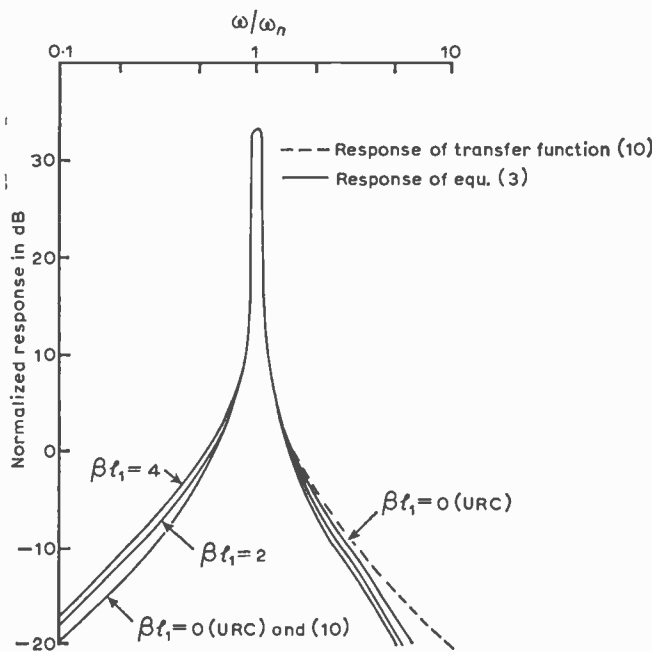


Fig. 2. Normalized responses of eqns. (3) and (10) for different values of  $\beta l_1$  (a)  $\delta = 89.4^\circ$ , (b)  $\delta = 87.14^\circ$ .

which yields for  $(RC)_2$

$$(RC)_2 = \frac{1}{4 + (\beta l_1/\pi)^2} (RC)_1 \quad \dots\dots(20)$$

It will be shown that the above approximation is adequate even for a value of  $\beta l_1$  as great as 4. Of course, if more accurate results are required for a particular application equation (16) may be solved by numerical methods.

The poles of the network of Fig. 1 are given by

$$\exp(-\beta l_1) \left\{ \cosh \theta_1 + (\beta l_1) \frac{\sinh \theta_1}{\theta_1} \right\} - k_1 = 0 \quad \dots\dots(21)$$

where

$$\theta_1 = \sqrt{(\beta l_1)^2 + z}, \quad z = x + jy = s(RC)_1 \quad \dots\dots(22)$$

It is known that the loci of the complex zeros of equation (21) are approximately parabolas (there is negligible numerical error), of the form,

$$y^2 = \frac{y_c^2}{|x_b|} (x + |x_b|) \quad \dots\dots(23)$$

where

$-|x_b|$  = the break frequency, the frequency at which there is a transition of the dominant zeros of equation (21) from real to complex,

and

$\pm y_c$  = the crossover frequencies, the frequencies at which the dominant complex zeros cross the  $y$  axis.

A method of determining  $|x_b|$  and  $y_c$ , as well as the values for various values of  $(\beta l_1)$  may be found elsewhere.<sup>4</sup>

Now for a given pole angle  $\delta$ , ( $0 \leq \delta < 90^\circ$ ),

$$\tan \delta = y/(-x), \quad \dots\dots(24)$$

and the dominant zeros of equation (21) may be found from equations (23) and (24) as,<sup>4</sup>

$$x = \frac{(y_c^2/|x_b|) - \sqrt{(y_c^2/|x_b|)^2 + 4y_c^2 \tan^2 \delta}}{2 \tan^2 \delta} \quad \dots\dots(25a)$$

$$y = -x \tan \delta \quad \dots\dots(25b)$$

$$\omega_{nz} = \sqrt{x^2 + y^2} \quad \dots\dots(25c)$$

The corresponding value of  $k_1$  is given by<sup>4</sup>

$$k_1 = \exp(-\beta l_1) \operatorname{Re} \left\{ \cosh \theta_1 + (\beta l_1) \frac{\sinh \theta_1}{\theta_1} \right\} \quad \dots\dots(26)$$

where

$$\theta_1 = \sqrt{(\beta l_1)^2 + x(1 - j \tan \delta)}$$

The approximation of the second-order band-pass function given by equation (10) is carried out as follows:

- (i) for a chosen  $\beta l_1$  determine<sup>4</sup> the corresponding values of  $|x_b|$  and  $y_c$ ,
- (ii) using the values of  $|x_b|$  and  $y_c$ , find  $x$  and  $y$  and, hence,  $\omega_{nz}$  from equation (25),
- (iii) once  $x$  and  $y$  are known find  $k_1$  from equation (26),
- (iv) choose the product  $(r_{01} c_{01} l_1^2) = (RC)_1$  to match the given pole positions with those of the dominant poles in the  $s$  plane,
- (v) choose  $k_2 = 0.5$ ,
- (vi) find  $(RC)_2$  using equation (20).

The normalized frequency responses of the network of Fig. 1 and that of the second-order band-pass function equation (10) are given for  $\delta = 89.4^\circ$  ( $Q \simeq 50$ ) in Fig. 2(a) and for  $\delta = 87.14^\circ$  ( $Q \simeq 10$ ) in Fig. 2(b) for three different values of  $\beta l_1$ . It may be seen that there is a close fit between the two responses in the pass band even for a value of  $\beta l_1$  as great as 4. Hence, the approximations involved in the pole-zero cancellation are justifiable.

Table 1 gives a listing of pertinent design data for various values of  $\beta l_1$ , and  $\delta = 89.4^\circ$  and  $\delta = 87.14^\circ$ . It may be seen that the magnitude of the amplifier gain  $k_1$  may be reduced considerably by increasing the taper  $\beta l_1$  of the ERC.

**Table 1**  
Design data for band-pass example

$\beta l_1$	$\delta^\circ$	$k_1$	$(RC)_2(RC)_1$	$\omega_{nz}$	Maximum $ T(j\omega) $	$Q$ Sensitivity
0	89.4	-11.22	0.25	19.534	213.59	30.74
	87.14	-9.9485	0.25	18.798	42.47	6.70
1	89.4	-6.312	0.2438	22.128	115.40	30.68
	87.14	-5.594	0.2438	21.389	23.00	6.65
2	89.4	-4.228	0.2270	25.733	74.69	30.64
	87.14	-3.745	0.2270	24.992	14.914	6.61
3	89.4	-3.191	0.2036	30.08	55.39	30.60
	87.14	-2.825	0.2036	29.34	11.06	6.57
4	89.4	-2.606	0.1779	34.96	45.34	30.55
	87.13	-2.307	0.1779	34.21	9.047	6.53

$$k_2 = 0.5$$

**3. Simultaneous Realization of Pairs of Complex Poles and Zeros**

Ghausi and Bello<sup>1</sup> have proposed the network shown in Fig. 3, where  $\mathcal{L}$  is a URC to realize the transfer function

$$T(s) = \frac{A+a}{A+b} \quad \dots\dots(27)$$

where

$$A = \cosh \theta = \cosh \sqrt{sRC} \quad \dots\dots(28a)$$

$$a = \frac{k_1(1-k_2)}{(1-k_1)} \quad \dots\dots(28b)$$

$$b = \frac{k_1}{1-k_1} \quad \dots\dots(28c)$$

and also propose cascading the network of Fig. 3 with itself giving

$$T_a(s) = \frac{A_1+a_1}{A_1+b_1} \cdot \frac{A_2+a_2}{A_2+b_2} \quad \dots\dots(29)$$

where

$$A_1 = \cosh \theta_1 = \cosh \sqrt{s(RC)_1} \quad \dots\dots(30a)$$

$$A_2 = \cosh \theta_2 = \cosh \sqrt{s(RC)_2} \quad \dots\dots(30b)$$

Ghausi and Bello claim that  $T_a(s)$  should approximate

$$T(s) = \frac{A_1+a_1}{A_2+b_2} \quad \dots\dots(31)$$

providing the dominant zeros of  $(A_1+b_1)$  and  $(A_2+a_2)$  cancel. However, it may be shown that equation (31) has a pole at infinity if  $(RC)_1 > (RC)_2$ , a zero at infinity if  $(RC)_1 < (RC)_2$ , or is equal to unity at infinity if  $(RC)_1 = (RC)_2$ . Hence, equation (29) cannot approximate equation (31) at high frequencies, except in the special case  $(RC)_1 = (RC)_2$ .

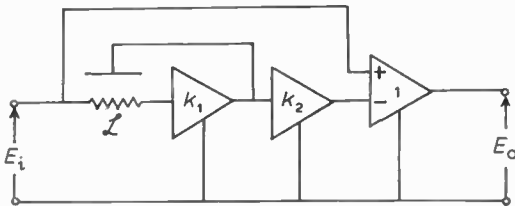


Fig. 3. Network proposed by Ghausi and Bello<sup>1</sup>.

**4. Proposed Structures and their Sensitivities**

Consider the networks of Figs 4(a) and (b), hereafter referred to as structures 1 and 2 respectively, where  $\mathcal{L}$  is an ERC with distributions

$$r(x) = r_0 e^{2\beta x}, \quad c(x) = c_0 e^{-2\beta x}, \quad (0 \leq x \leq l) \quad (32)$$

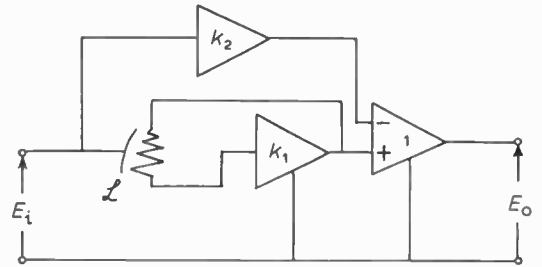
The transfer function for these two structures is given by

$$T(s) = H \frac{A+a}{A+b} \quad \dots\dots(33)$$

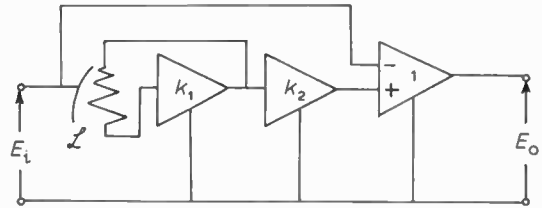
where

$$A = e^{-\beta l} \left\{ \cosh \theta + (\beta l) \frac{\sinh \theta}{\theta} \right\} \quad \dots\dots(34)$$

$$\theta = \sqrt{(\beta l)^2 + s(r_0 c_0 l^2)}$$



(a) Structure 1,



(b) Structure 2.

Fig. 4. Proposed structures to realize equation (33).

and

$$a = \frac{k_1(k_2-1)}{k_1-k_2} \quad \dots\dots(35a)$$

$$b = -k_1 \quad \dots\dots(35b)$$

$$H = (k_1-k_2) \quad \dots\dots(35c)$$

for structure 1, while for structure 2

$$a = \frac{k_1(1-k_2)}{k_1 k_2 - 1} \quad \dots\dots(36a)$$

$$b = -k_1 \quad \dots\dots(36b)$$

$$H = k_1 k_2 - 1 \quad \dots\dots(36c)$$

Hence, for structure 1

$$k_1 = -b, \quad k_2 = \frac{b(a+1)}{b-a} \quad \dots\dots(37)$$

while for structure 2

$$k_1 = -b, \quad k_2 = \frac{b-a}{b(a+1)} \quad \dots\dots(38)$$

Consider the sensitivities of structures 1 and 2 with respect to  $k_1$ . Since  $b = -k_1$  for both these structures, any sensitivity function with respect to  $k_1$  is

$$S_{k_1} = \frac{k_1}{b} \frac{\partial b}{\partial k} S_b = S_b \quad \dots\dots(39)$$

Also, for the network of Fig. 3 it is known that

$$b = \frac{k_1}{1-k_1} \quad \dots\dots(40)$$

from equation (28c). Hence

$$S_{k_1} = \frac{k_1}{b} \frac{\partial b}{\partial k_1} S_b = \frac{1}{1-k_1} S_b \quad \dots\dots(41)$$

To realize a given complex pole-pair the factor  $b$  is the same for all the structures. But  $k_1$  in equation (41) is close to unity for the network of Fig. 3; hence, from equations (39) and (41) we see that the sensitivities with

respect to  $k_1$  for structures 1 and 2 are very much lower than those for the structure of Ghauri and Bello.

To make a comparison of the sensitivities, suppose the lines used in all the structures are URCs. If the network of Fig. 3 were used to realize a pole-pair of even moderate  $Q$ , say  $Q = 10$ ,  $k_1$  is approximately  $0.9^3$ . Hence,  $S_{k_1}$  for the structure of Fig. 3 is about 10 times that for the structures 1 and 2 even for this moderate  $Q$ . However, it should be noted that inverting higher gain amplifiers must be used in structures 1 and 2; but we know from the previous band-pass realization that by employing ERCs instead of URCs in these structures, the gain  $k_1$  may be considerably reduced.

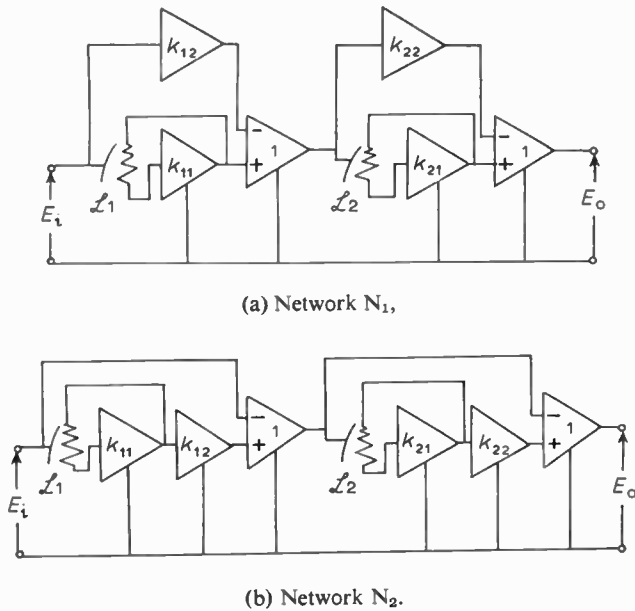


Fig. 5. Proposed structures to realize equation (44).

5. Design Equations and Procedure for Realizing Complex Poles and Zeros

Consider a cascade of structure 1 with itself as in Fig. 5(a) or of structure 2 with itself as in Fig. 5(b); these networks will be called  $N_1$  and  $N_2$  respectively. In both these networks  $\mathcal{L}_1$  and  $\mathcal{L}_2$  are ERCs with distributions,

$$\mathcal{L}_1: \begin{cases} r_1(x) = r_{01} \exp(2\beta_1 x) \\ c_1(x) = c_{01} \exp(-2\beta_1 x) \end{cases} \quad (0 \leq x \leq l_1) \quad \dots(42)$$

$$\mathcal{L}_2: \begin{cases} r_2(x) = r_{02} \exp(2\beta_2 x) \\ c_2(x) = c_{02} \exp(-2\beta_2 x) \end{cases} \quad (0 \leq x \leq l_2) \quad \dots(43)$$

Then the transfer function of the networks is

$$T(s) = H \frac{A_1 + a_1}{A_1 + b_1} \cdot \frac{A_2 + a_2}{A_2 + b_2} \quad \dots(44)$$

where

$$A_1 = \exp(-(\beta l)_1) \left\{ \cosh \theta_1 + (\beta l)_1 \frac{\sinh \theta_1}{\theta_1} \right\}$$

$$A_2 = \exp(-(\beta l)_2) \left\{ \cosh \theta_2 + (\beta l)_2 \frac{\sinh \theta_2}{\theta_2} \right\}$$

$$\theta_1 = \sqrt{(\beta l)_1^2 + s(r_{01} c_{01} l_1^2)} = \sqrt{(\beta l)_1^2 + s(RC)_1}$$

$$\theta_2 = \sqrt{(\beta l)_2^2 + s(r_{02} c_{02} l_2^2)} = \sqrt{(\beta l)_2^2 + s(RC)_2}$$

Also for network  $N_1$

$$k_{11} = -b_1, \quad k_{12} = \frac{b_1(a_1 + 1)}{(b_1 - a_1)} \quad \dots(45a)$$

$$k_{21} = -b_2, \quad k_{22} = \frac{b_2(a_2 + 1)}{b_2 - a_2} \quad \dots(45b)$$

$$H = (k_{11} - k_{12})(k_{21} - k_{22}) \quad \dots(45c)$$

While for network  $N_2$

$$k_{11} = -b_1, \quad k_{12} = \frac{(b_1 - a_1)}{b_1(a_1 + 1)} \quad \dots(46a)$$

$$k_{21} = -b_2, \quad k_{22} = \frac{(b_2 - a_2)}{b_2(a_2 + 1)} \quad \dots(46b)$$

$$H = (k_{11} k_{12} - 1)(k_{21} k_{22} - 1) \quad \dots(46c)$$

The dominant zeros of  $(A_1 + a_1)$  will be used to realize the given complex zeros and the dominant zeros of  $(A_2 + b_2)$  to realize the given complex poles. It is also desirable to cancel the dominant zeros of  $(A_1 + b_1)$  with those of  $(A_2 + a_2)$  since they will lie within the frequency range of interest. Because of stability considerations, we shall fix the dominant zero of  $(A_1 + b_1)$  in the  $\{s(RC)_1\}$ -plane and then choose  $a_2$  such that the dominant zero of  $(A_2 + a_2)$  cancels that of  $(A_1 + b_1)$  in the  $s$ -plane. Both dominant zeros should lie on the negative real axis, otherwise cancellation will not be possible except in the special case when  $(RC)_1 = (RC)_2$ .

Let

$$s_p(RC)_1 = x_p \quad \dots(47)$$

where  $s_p$  is the dominant zero of  $(A_1 + b_1)$ . Since  $s_z$ , the dominant zero of  $(A_2 + a_2)$  lies on the negative real axis, the following inequality applies,

$$0 \leq |s_z(RC)_2| \leq |(x_b)_2| \quad \dots(48)$$

where  $-(x_b)_2$  is the break frequency as defined by equation (23). For cancellation,  $s_p = s_z$  and, hence, from equations (47) and (48) we have

$$0 \leq \frac{(RC)_2}{(RC)_1} \leq \frac{|(x_b)_2|}{|x_p|} \quad \dots(49)$$

For as large a range of  $(RC)_2/(RC)_1$  as possible,  $x_p$  should be chosen as near the origin as possible.

Once a value of  $x_p$  has been decided upon,  $b_1$  can be found from the equation

$$b_1 = -\exp(-(\beta l)_1) \left\{ \cosh \theta_{10} + (\beta l)_1 \frac{\sinh \theta_{10}}{\theta_{10}} \right\} \quad \dots(50a)$$

where

$$\theta_{10} = \sqrt{(\beta l)_1^2 + x_p} \quad \dots(50b)$$

The corresponding value of  $a_2$  can be found from

$$a_2 = -\exp(-(\beta l)_2) \left\{ \cosh \theta_{20} + (\beta l)_2 \frac{\sinh \theta_{20}}{\theta_{20}} \right\} \quad \dots(51a)$$

where

$$\begin{aligned} \theta_{20} &= \sqrt{(\beta l)_2^2 + s_z(RC)_2} \\ &= \sqrt{(\beta l)_2^2 + x_p \{(RC)_2/(RC)_1\}} \quad \dots(51b) \end{aligned}$$

The ratio  $(RC)_2/(RC)_1$  may be determined from the positions of the complex poles and zeros.

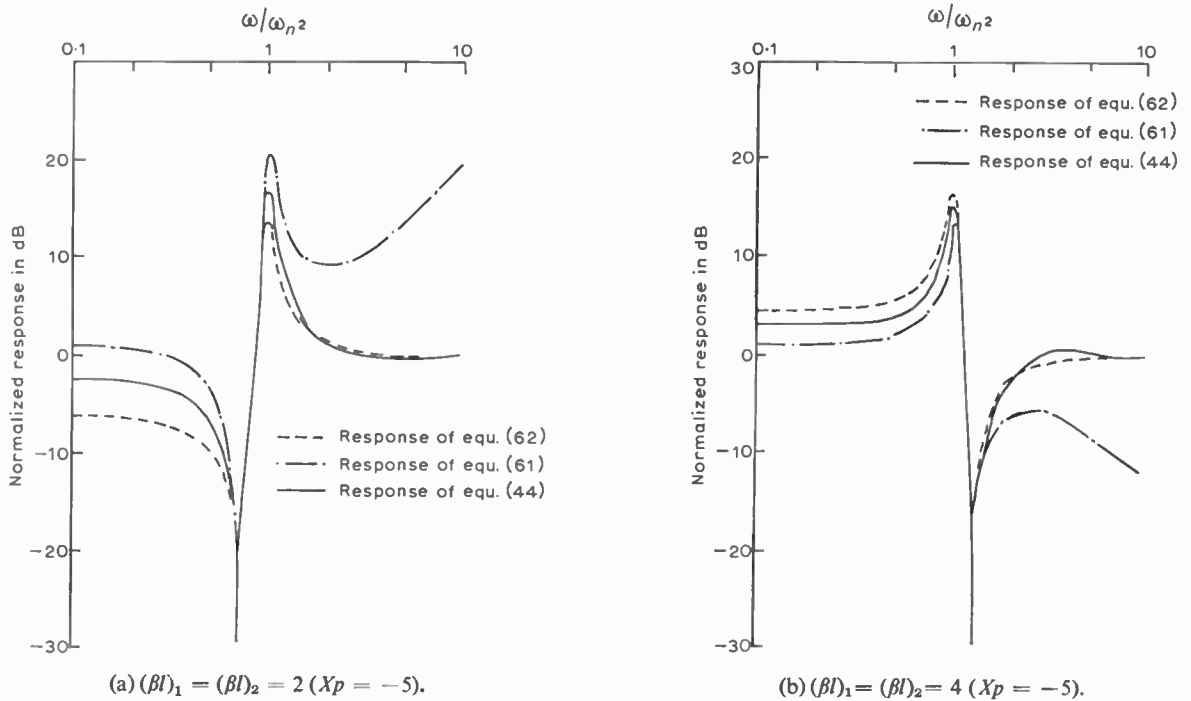


Fig. 6. Normalized responses for a pole angle  $\delta_2 = 87.14^\circ$  and zero angle  $\delta_1 = 90^\circ$ .

Assume the required complex zero locations are  $s_1, s_1^* = \sigma_1 \pm j\omega_1$  and the required pole locations are  $s_2, s_2^* = \sigma_2 \pm j\omega_2$ . Let

$$x_1 + jy_1 = z_1 = s_1(RC)_1 \quad \dots\dots(52)$$

and

$$x_2 + jy_2 = z_2 = s_2(RC)_2 \quad \dots\dots(53)$$

Also let

$$\omega_{n1} = \sqrt{\sigma_1^2 + \omega_1^2} \quad \dots\dots(54)$$

$$\omega_{n2} = \sqrt{\sigma_2^2 + \omega_2^2} \quad \dots\dots(55)$$

$$\omega_{nz1} = \sqrt{x_1^2 + y_1^2} \quad \dots\dots(56)$$

$$\omega_{nz2} = \sqrt{x_2^2 + y_2^2} \quad \dots\dots(57)$$

Then

$$\frac{(RC)_2}{(RC)_1} = \frac{\omega_{n1} \omega_{nz2}}{\omega_{n2} \omega_{nz1}} \quad \dots\dots(58)$$

The given poles and zeros may now be realized using network  $N_1$  or  $N_2$  (or a combination of both), as follows:

Zeros

- (i) For a chosen  $(\beta l)_1$  determine the corresponding values of  $|(x_b)_1|$  and  $(y_c)_1$ .<sup>4</sup>
- (ii) Using the values of  $|(x_b)_1|$ , and  $(y_c)_1$  and the zero angle  $\delta_1$ , find  $x_1$  and  $y_1$  from (25) and  $\omega_{nz1}$  from equation (56).
- (iii) Once  $x_1$  and  $y_1$  are known,  $a_1$  may be determined as

$$a_1 = -\exp(-(\beta l)_1) \times \text{Re} \left\{ \cosh \theta_{11} + (\beta l)_1 \frac{\sinh \theta_{11}}{\theta_{11}} \right\} \quad \dots\dots(59)$$

where

$$\theta_{11} = \sqrt{(\beta l)_1^2 + x_1(1 - j \tan \delta_1)}$$

- (iv) For a chosen  $x_p$  find  $b_1$  from equation (50).
- (v) Determine the amplifier gains  $k_{11}$  and  $k_{12}$  from (45a) for network  $N_1$  or from equation (46a) for network  $N_2$ .

Poles

- (i) For a chosen  $(\beta l)_2$  determine  $|(x_b)_2|$  and  $(y_c)_2$ .<sup>4</sup>
- (ii) Using the values of  $|(x_b)_2|$ ,  $(y_c)_2$  and the pole angle  $\delta_2$ , find  $x_2$  and  $y_2$  from (25) and  $\omega_{nz2}$  from equation (57).
- (iii) Once  $x_2$  and  $y_2$  are known,  $b_2$  may be determined as

$$b_2 = -\exp(-(\beta l)_2) \times \text{Re} \left\{ \cosh \theta_{21} + (\beta l)_2 \frac{\sinh \theta_{21}}{\theta_{21}} \right\} \quad \dots\dots(60)$$

where

$$\theta_{21} = \sqrt{(\beta l)_2^2 + x_2(1 - j \tan \delta_2)}$$

- (iv) Find  $(RC)_2/(RC)_1$  from equation (58) and  $a_2$  from equation (51).
- (v) Determine the amplifier gains  $k_{21}$  and  $k_{22}$  from equation (45b) for network  $N_1$  or equation (46b) for network  $N_2$ .
- (vi) Choose the product  $(RC)_1$  or  $(RC)_2$  to match the given zero (or pole) positions with those of the dominant zeros (or poles) in the  $s$ -plane.

To illustrate the fact that the poles and zeros are realized to a good approximation, the normalized frequency response of equation (44) is plotted in Fig. 6(a) for a pole angle  $\delta_2 = 87.14^\circ$  ( $Q \approx 10$ ) and a pair of  $j\omega$

Table 2

Design data for example realizing a pair of complex poles and a pair of complex zeros

$(\beta l)_1$ $(\beta l)_2$	$\delta_1^\circ$	$\delta_2^\circ$	$\omega_{n1}/\omega_{n2}$	$(RC)_2/(RC)_1$	Network $N_1$	Network $N_2$
2	90	87.14	0.7	0.6744	$k_{11} = 0.3009$ $k = 0.3459$ $k_{21} = -3.745$ $k_{22} = 0.4609$ $H = 0.1895$	$k_{11} = 0.3009$ $k_{12} = 2.891$ $k_{21} = -3.745$ $k_{22} = 2.170$ $H = 1.188$
4	90	87.14	1.3	1.265	$k_{11} = 0.5569$ $k_{12} = 0.6328$ $k_{21} = -2.3067$ $k_{22} = 0.4407$ $H = 0.2086$	$k_{11} = 0.5569$ $k_{12} = 1.580$ $k_{21} = -2.3067$ $k_{22} = 2.267$ $H = 0.7480$

$$x_p = -5$$

axis zeros ( $\delta_1 = 90^\circ$  and a zero to pole frequency ratio ( $\omega_{n1}/\omega_{n2}$ ) of 0.7. Here we have chosen  $(\beta l)_1 = (\beta l)_2 = 2$ . Figure 6(b) shows the normalized frequency response of equation (44) with all the parameters the same as before, but the zero to pole frequency ratio is 1.3 and  $(\beta l)_1 = (\beta l)_2 = 4$ . Also, in these figures the frequency responses of

$$\frac{A_1 + a_1}{A_2 + b_2} \quad \dots\dots(61)$$

and that of the biquadratic function

$$\frac{s^2 + \omega_{n1}^2}{s^2 + 2\omega_{nz} \cos(\delta_2)s + \omega_{n2}^2} \quad \dots\dots(62)$$

are plotted for purposes of comparison. It may be observed that networks  $N_1$  and  $N_2$  realize, to a good approximation, the response of equation (62). The gains of the different amplifiers and other design data for these realizations are given in Table 2.

## 6. Conclusions

New structures utilizing ERCs have been given and detailed design procedures are indicated for realizing band-pass transfer functions and transfer functions containing a pair of complex poles and a pair of complex zeros. It has been shown that in the case of the band-pass filter, the frequency response very closely approximates a second-order band-pass transfer function. It has also been shown that the amplifier gains may be reduced by increasing the taper of the ERC and that for the structures realizing complex zeros and poles, any of the

sensitivity functions with respect to the gain of the pole determining amplifier, is lower than that for the structure proposed by Ghauri and Bello.

## 7. Acknowledgments

This work was supported under the National Research Council of Canada, Grant A-7313, and is based on a portion of a Ph.D. thesis submitted by J. Walsh under the supervision of Professor M. N. S. Swamy.

## 8. References

1. Ghauri, M. S. and Bello, V. G., 'Active distributed RC realizations of low-pass magnitude specifications', *Trans I.E.E.E. on Circuit Theory*, CT-16, pp. 346-358, August 1969.
2. Kerwin, W. J., 'Synthesis of active RC networks containing lumped and distributed elements', *Proc. First Asilomar Conference on Circuits and Systems*, pp. 288-298, November 1967.
3. Walsh, J. and Swamy, M. N. S., 'Design of active distributed RC low-pass filters using exponential lines', *Electronics Letters*, 6, pp. 293-295, 30th April 1970.
4. Swamy, M. N. S. and Walsh, J., 'A simple design procedure for active low-pass filters using exponential RC lines', *Proc. Thirteenth Midwest Symposium on Circuit Theory*, pp. X.6.1-X.6.10 May 1970.
5. Walsh, J., Giguere, J. C. and Swamy, M. N. S., 'Active filter design using exponentially tapered RC-lines', *Trans I.E.E.E. on Circuit Theory*, CT-17, pp. 645-648, November 1970.

Manuscript received by the Institution on 13th March 1972 (Paper No. 1472/CC146).

© The Institution of Electronic and Radio Engineers, 1972

# A Formal Method for Designing Sequential Circuits from Synchronous Flip-Flops such as the J-K Type using a Hybrid Synchronous-Asynchronous Technique

H. DUNDERDALE, B.Sc.Tech.\*

## SUMMARY

A formal method is presented which simplifies the realization of many counter sequences in asynchronous form from synchronous flip-flops such as the J-K or D type, without requiring the use of preset or clear connexions to establish the sequence. The method is demonstrated by using the procedure to obtain asynchronous circuits in terms of J-K flip-flops for counters operating in the 8-4-2-1 and 5-4-2-1 b.c.d. codes. Though circuits for these sequences are well known the design procedure is of educational interest and offers alternative circuits for the sequences. The procedure is equally applicable to the realization of many other sequences.

\*Electrical Engineering Department, University of Salford, Salford M5 4WT.

## 1. Introduction

A paper by Deant† describes a method by which synchronous parallel counters can be designed to follow any desired sequence. In this short contribution the method is extended to the design of asynchronous counter circuits in terms of synchronous J-K flip-flops. Asynchronous circuits have the advantage of normally requiring less overall hardware than their synchronous counterparts and in addition may require a less powerful drive source since less stages need to be driven by the input signal.

## 2. Design Method

The basic principle of the method is to design each stage of the asynchronous counter on a synchronous basis by using clock sources derived from the output changes of lesser significant stages. For many sequences the required output of a given stage will be readily recognized as realizable from a simple counter-connected flip-flop. The initial design procedure will, therefore, be concerned with the elimination of stages that only require such counter connexions. The design of the remaining stages requires the recognition of unipolarity changes of lesser significant stages which can be used as clock sources to activate more significant stages. The design of the feedback logic to the J- and K-inputs of these stages is based on the principles described in the cited reference.

The design procedure is best described as a sequence of steps:

- Step 1 Tabulate the sequence.
- Step 2 Recognize stages which have simple binary counter action and design accordingly.
- Step 3 Choose suitable clock sources for the trigger inputs of the remaining stages by ascertaining whether changes in output of the stage under consideration are covered by unipolarity changes in output of a lesser significant stage.
- Step 4 Construct Karnaugh maps to minimize the required feedback logic taking full advantage of the logical properties of the basic synchronous flip-flop to be utilized.

## 3. Application of the Design Procedure to the Design of an 8-4-2-1 B.C.D. Asynchronous Up-counter Circuit

Assume that the design is to be based on J-K flip-flops which conform to the truth table shown in Table 1, in which the convention is that Q— and Q are respectively the states of the Q-output of the flip-flop before and after the 1 → 0 edge of the clock source. An examination of the 8-4-2-1 b.c.d. sequence shown in Table 3 reveals that the *d*-column sequence can be realized by connecting the T-terminal of a counter connected J-K flip-flop to the input signal, the counter connexion being achieved by connecting the J- and K-terminals to logical unity, and

† Dean, K. J., 'The design of parallel counters using the map method', *The Radio and Electronic Engineer*, 32, pp. 159-62, September 1966.

**Table 1.** Truth table for the J-K flip-flops considered in the design examples

J	K	Q
0	0	$Q^-$
0	1	0
1	0	1
1	1	$\overline{Q^-}$

**Table 4.** Karnaugh-Veitch maps for the input logic of the A and C stages of the 8-4-2-1 b.c.d. counters

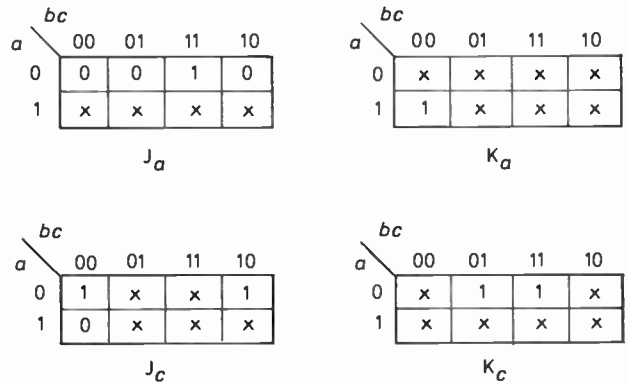


**Table 2.** Sufficient conditions at the J and K entries to achieve the required Q-output transitions

Required output change		Required input values	
$Q^- \rightarrow Q$		J	K
0	0	0	x
1	1	x	0
1	0	x	1
0	1	1	x

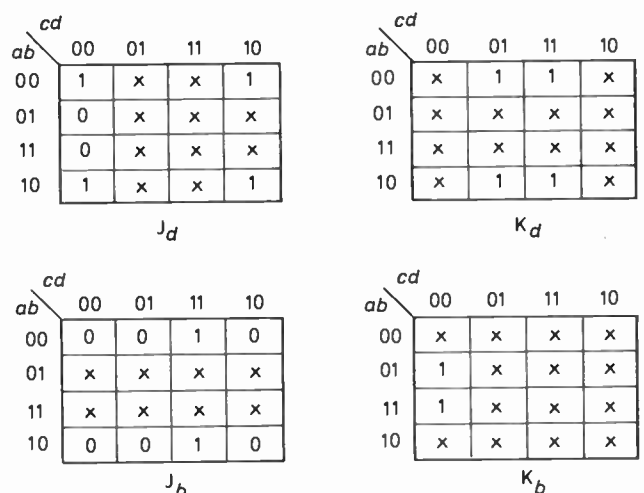
**Table 5.** 5-4-2-1 b.c.d. sequence

	5	4	2	1
	a	b	c	d
0	0	0	0	0
1	0	0	0	1
2	0	0	1	0
3	0	0	1	1
4	0	1	0	0
5	1	0	0	0
6	1	0	0	1
7	1	0	1	0
8	1	0	1	1
9	1	1	0	0

**Table 3.** Table showing the 8-4-2-1 b.c.d. sequence with arrows inserted to indicate the clock edge source for stages A and C

	8	4	2	1
	a	b	c	d
0	0	0	0	0
1	0	0	0	1
2	0	0	1	0
3	0	0	1	1
4	0	1	0	0
5	0	1	0	1
6	0	1	1	0
7	0	1	1	1
8	1	0	0	0
9	1	0	0	1

**Table 6.** Minimization maps for the input logic to the B and D stages of the 5-4-2-1 counter



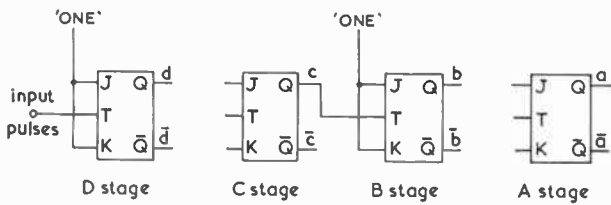


Fig. 1. Circuit of the 8-4-2-1 b.c.d. counter after the initial design stage.

that the *b* column sequence can be achieved by driving the T-terminal of a similarly counter connected stage with the Q-output of the C-stage. The circuit at this stage of design is as shown in Fig. 1.

An inspection of the b.c.d. sequence of Table 2 shows that the Q-output of the D-stage can be used as a clock source for stages A and C since 1 → 0 changes of the *d*-column cover all changes of the *a* and *c* columns. (To aid the appreciation of this fact arrows are inserted in the relevant positions of Table 3.) Entries are made in the Karnaugh-Veitch maps of Table 4 which take advantage of the sufficient conditions to achieve a desired transition displayed in Table 2. Since the values of *a*, *b* and *c* do not repeat at any of the sample points, maps for three variables are adequate. Required change of state J-K entries are only made for values of *a, b, c*, corresponding to 000, 001, 010, 011 and 100, all other entries taking 'don't care' values. The map minimization gives:

$$J_a = bc \quad K_a = 1 \quad \text{or} \quad K_a = a \quad \text{or} \quad K_a = \bar{b}$$

$$J_c = \bar{a} \quad K_c = 1 \quad \text{or} \quad K_c = \bar{a} \quad \text{or} \quad K_c = \bar{b}$$

If J-K flip-flops which include an input AND gate are available then a suitable form for the final circuit would be that shown in Fig. 2, otherwise since

$$J_a = bc = \bar{b} + \bar{c}$$

then the AND gate can be replaced by a NOR gate with inputs supplied from the Q-outputs of the B and C stages.

In the circuit given in Fig. 2 where a choice existed for a K-input the logical value unity has been selected in preference to a variable on the grounds that this arrangement reduced the circuitry exposed to transient conditions. In other cases where a choice existed between single variables for a required input the selection would be influenced by considerations of circuit layout or the frequency with which a given variable changes.

It will be observed that the frequency of the clock source derived from the first stage of the 8-4-2-1 counter

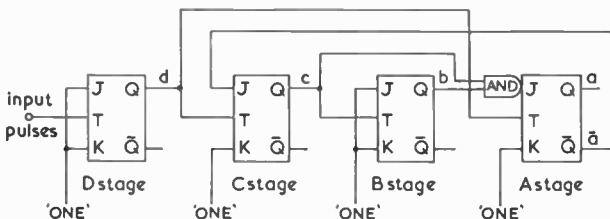


Fig. 2. Completed circuit for the 8-4-2-1 b.c.d. counter.

circuit is half that of the input frequency. This enables the asynchronous version to operate at a higher count rate than the synchronous version, in which every stage is clocked at the input signal frequency and in which the input logic values to several stages are dependent on changes of the least significant bit stage outputs.

#### 4. Application of the Design Procedure to the Design of a 5-4-2-1 Counter Circuit

As a further example of the design procedure consider now the design of a circuit to give the 5-4-2-1 sequence of Table 5. In this case stages A and C are immediately recognized as requiring simple counter connexions since changes of the *a* column coincide with 1 → 0 changes of the *b* column, and changes of the *c* column coincide with 1 → 0 changes of the *d* column. Thus stages A and C are wired in the counter-connected mode and driven respectively at the T terminals by the Q-outputs of the B and D stages. The input signal is a suitable clock source for stages B and D since 1 → 0 changes

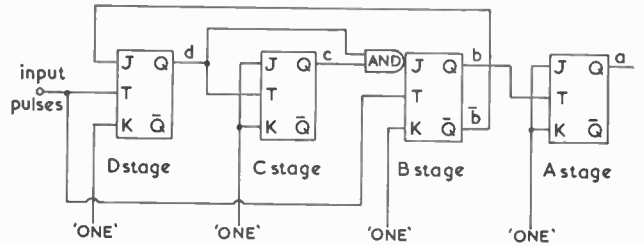


Fig. 3. Completed circuit for the 5-4-2-1 b.c.d. counter.

of the input signal cover all changes in output of these stages. Stages B and D are now designed on a synchronous basis using this clock source, giving the maps of Table 6 from which

$$J_d = \bar{b} \quad K_d = 1 \quad \text{or} \quad K_d = \bar{b} \quad \text{or} \quad K_d = d$$

$$J_b = cd \quad K_b = 1 \quad \text{or} \quad K_b = b \quad \text{or} \quad K_b = \bar{c}$$

The values selected for the circuit of Fig. 3 are chosen according to the same criterion as used for the design of the 8-4-2-1 counter.

#### 5. Conclusions

A hybrid technique for asynchronous design has been demonstrated which is much faster than the procedure required for a full asynchronous treatment. Though circuits for the 8-4-2-1 and 5-4-2-1 sequences are well known, the technique is of educational interest and the procedure could be applied to the realization of other sequences. Equally the procedure could be used in design in terms of other synchronous flip-flops such as the D-type, though in the latter case the required input logic would be more complex. An additional advantage of the technique is that the use of preset or clear connexions is not required in determining a sequence.

Manuscript received by the Institution on 2nd May 1972. (Short Contribution No. 157/147C.)

© The Institution of Electronic and Radio Engineers, 1972

# A Pseudo-Random Pulse Train Generator with Controllable Rate for Modelling of Audiometric Systems

J. K. MOSS, B.Sc.,\*

R. J. SIMPSON, B. Tech., M.Sc.\*

and

W. TEMPEST, Ph.D.†

## SUMMARY

Design details are given of a pseudo-random pulse train generator. The generator produces a sequence of '0' and '1' pulses which occur at uniform time intervals, and with a controllable average rate of '0's to '1's, but in which the detailed distribution of '0's and '1's is essentially random. The system is such that the output pattern can be repeated. The instrument has been developed to simulate the behaviour of a human listener's response to sound in the region of the auditory threshold but may find applications in other simulations employing Monte Carlo methods, etc. The system is easily constructed and by using modern integrated circuits only a small number of packages is required.

\* Harris College, (proposed Preston Polytechnic), Preston, Lancashire,

† University of Salford, Salford M5 4WT, Lancashire.

## 1. Introduction

Random pulse generators are in wide use as aids to the solution of many engineering and scientific problems in fields as diverse as Monte Carlo simulation studies, psychophysics and radar technology. The generator discussed in this paper was developed as part of a hardware simulation to aid an investigation into optimum diagnostic test procedures for one aspect of deafness.

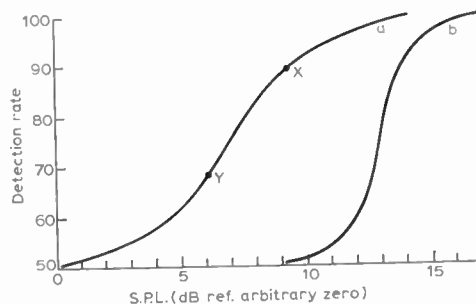


Fig. 1. Psychometric functions which are predicted a for a normal ear b for an ear with a cochlear disorder.

Figure 1 shows typical psychometric functions for (i) a normal ear and (ii) for an ear with an sensorineural loss. The curves shown relate percentage detection rate, in a two-interval forced choice (2-i.f.c.) experiment,<sup>1</sup> to sound pressure level (s.p.l.). The difference in slope between the normal and abnormal ears has a potential use in diagnosis.<sup>1</sup> In a diagnostic routine it is necessary to locate at least two points (such as X and Y on Fig. 1) in order to make an estimate of the slope. In practice this involves determining the s.p.l. corresponding to two specific detection rates.

There are several possible procedures in 2-i.f.c. experiments, and one of them, illustrated in Fig. 2, may be compared to a closed-loop control system in which the human subject forms part of the loop. In this system the desired detection rate is compared with the actual detection rate, and the resulting error is used to control the s.p.l.

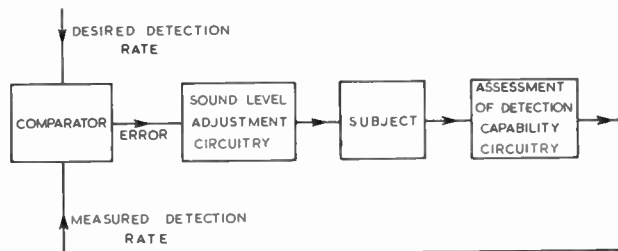


Fig. 2. Closed-loop representation of diagnostic routine.

One aspect of the present research programme is concerned with optimizing the method of determining the detection rate and this in turn implies optimizing the behaviour of the control loop. Repeated tests using a human subject present difficulties because the test is tedious and the subject becomes fatigued. In addition there is the possibility that the subject's performance may vary with time in an unknown manner. It therefore

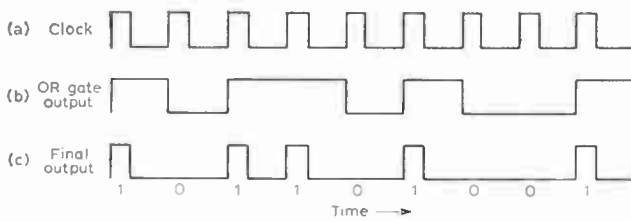


Fig. 3. Typical noise waveforms.

seemed that computer modelling might provide the best technique, offering the possibility of higher speeds and the facility for testing the effects of many detection criteria and other variable factors on the settling time of the loop.

A hardware simulation of the system shown in Fig. 2 requires a model of the subject, and in engineering terms this necessitates an instrument to produce a pulse train of the form shown in Fig. 3(c), where a '1' signifies a 'hit' (detection) and a '0' signifies absence of detection. Furthermore, whilst the resulting sequence should be apparently random, the ratio of '1's to '0's should be controllable by an input signal derived from the s.p.l. This is the instrument described and is basically a two level noise generator.

Early methods of approximating white noise used natural fluctuation phenomena. These have certain disadvantages, such as requiring complex control circuitry, and in recent years pseudo-random binary sequences employing chain code generators have been widely used,<sup>2-4</sup> although generators using natural fluctuation phenomena are still finding applications.<sup>5,6</sup> Pseudo-random generators have the advantage of repeatability of number sequences and predetermined statistics. When used for producing a two level signal of levels 0 and 1, both methods normally endeavour to make the probability of a '1' equal to the probability of a '0' at any sampling instant, i.e.  $P(0) = P(1) = \frac{1}{2}$ .

An extension to the basic noise generator, as required in the present application, is to produce a random binary sequence in which the average ratio of 1's to 0's may be varied. Once again different approaches are possible using either pseudo-random sequences<sup>7-11</sup> or natural fluctuation phenomena.<sup>6</sup> There now follows design details of a generator using pseudo-random sequences.

**2. Theoretical Background**

Consider two integer numbers  $R$  and  $F$  in the range 0 to  $(N-1)$ , i.e. the numbers have  $N$  possible values.  $R$  is a random number which has equal likelihood of being any number in the range 0 to  $(N-1)$ .  $F$  is a fixed number. The method compares  $R$  with  $F$  so that a '1' output is produced if  $R \geq F$ , otherwise a '0' is produced. It follows that for any value of fixed reference number  $F$ , the probability of an output is:

$$P = \frac{N-F}{N}$$

therefore the expected output rate  $\gamma = (N-F)/N$ . 100%. By changing the value of  $F$ , and by making  $N$  sufficiently large the output rate may be varied in fine steps.

The experiment for which the equipment was produced required the control in output rate to be better than 1%, and since binary techniques were used, 7-bit numbers for  $F$  and  $R$  were convenient. This allows 128 steps of control and  $F$  and  $R$  may take any integer value between 0 and 127. The system arrangement is then as shown in Fig. 4. The expected output rate then becomes

$$\gamma = \frac{128-F}{128} 100\% \dots\dots(1)$$

Alternatively, for a desired expected output rate, the value of fixed reference may be evaluated by re-arranging eqn. (1) giving

$$F = \frac{128(100-\gamma)}{100}$$

**3. Hardware Implementation**

Each of the three blocks in Fig. 4 will be considered in turn.

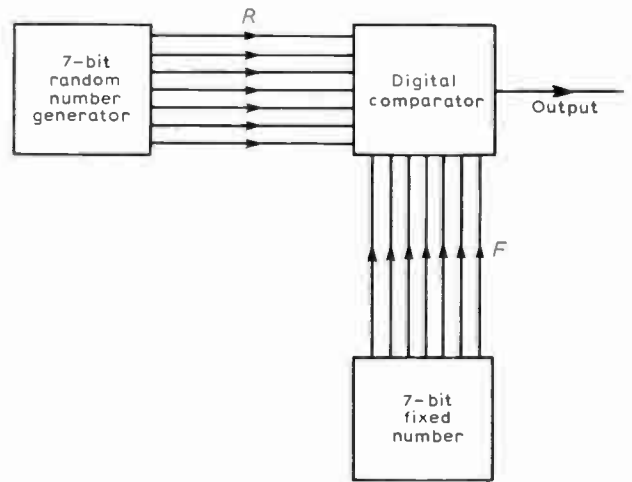


Fig. 4. Basic system block diagram of noise generator.

**3.1 Generator and Control Unit for 7-Bit Random Number**

**3.1.1 Basic generator**

Redshaw<sup>7</sup> and Robinson<sup>8</sup> have shown that a parallel  $n$ -bit pseudo-random number may be produced by combining the outputs of two prime chain code generators in an array of exclusive OR gates. The circuit shown in Fig. 5 enables a 7-bit number to be produced from 11- and 15-stage chain code generators. It has been argued<sup>7,8</sup> that in order to avoid problems of local non-randomness it is necessary to combine the outputs of two chain code generators, rather than use a single generator. The use of a single generator gives rise to difficulties since the output sequence of one stage is repeated at the next stage one clock pulse later. Even using two chain code generators care must be taken in the choice of connexions for combining the two chain codes, otherwise patterns produced at the output of a particular exclusive-OR may be a delayed version of a similar pattern from another exclusive-OR. Figure 5 shows the connexions for producing one 7-bit pseudo-random number. The circuit has the cap-

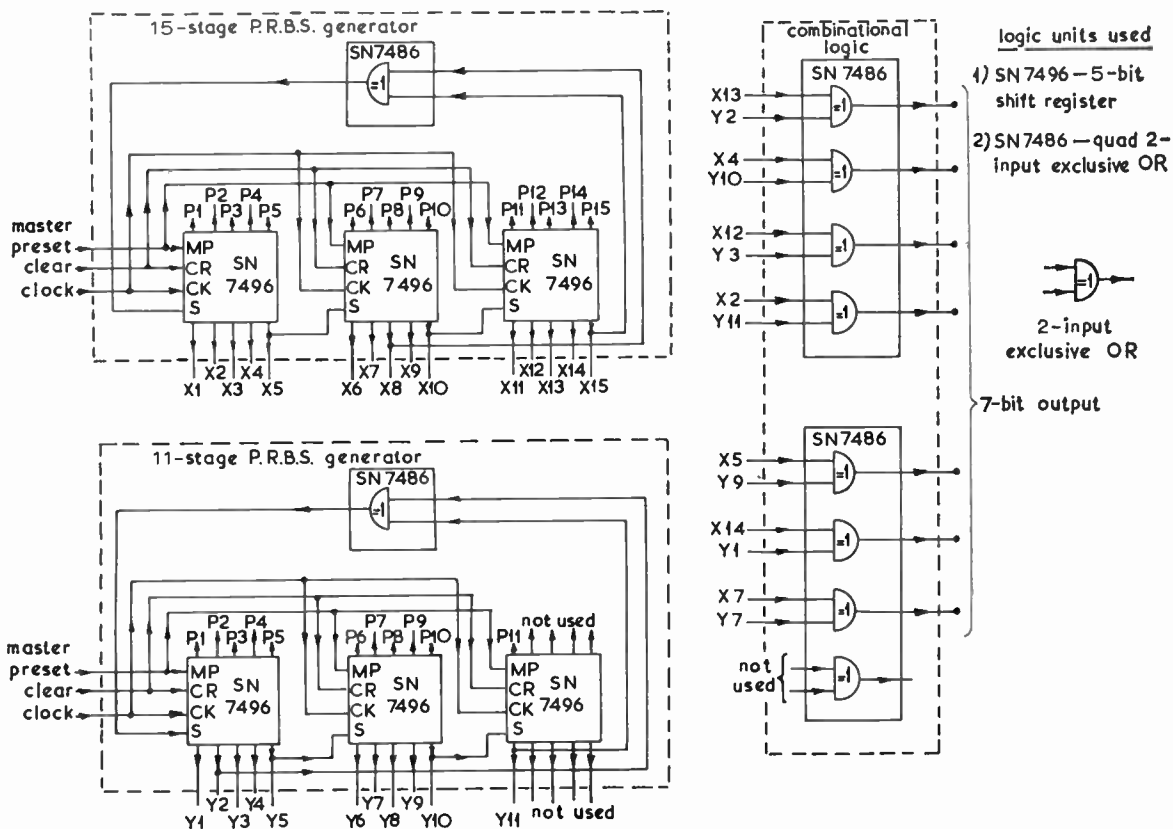


Fig. 5. 7-bit random number generator.

ability of simultaneously producing a second 7-bit pseudo-random number, the connexions of which are given in Appendix 1. Each SN7496 contains a 5-bit shift register with accessible output and preset terminals for each stage. Exclusive-OR feedback takes place in the SN7486 which is a quad two-input exclusive-OR gate.

It should be noted that a two-input exclusive-OR gate has the property of combining two random inputs, each of equal likelihood of being 1 or 0 and producing an output which also has an equal likelihood of being 1 or 0. Thus each bit of the 7-bit output has an equal chance of being 1 or 0 since the basic property of the chain code generator is that the output from any stage has an equal chance of being 1 or 0.†

### 3.1.2 Control unit

The SN7496 5-bit shift register has the following properties: (i) to clear each stage logic 0 must be applied to clear input, during normal operation apply logic 1; (ii) to preset the stages for any particular starting sequence the individual preset inputs should be set to 0 or 1 as desired. The sequence is then read into the registers by applying logic 1 to the master preset input. During normal operation the master preset input should be logic 0; (iii) shift occurs in the register when the clock input switches from logic 0 to logic 1.

† The actual number of 1's is  $(N+1)/2$  and number of 0's is  $(N-1)/2$  where  $N$  = sequence length, but if  $N \gg 1$  then  $p(1) = p(0) = \frac{1}{2}$ .

With the above in mind the control unit shown in Fig. 6 gives flexible operation of the circuit and has the following facilities:

- (i) The master presets to both 11- and 15-stage register is as explained in (ii) above.
- (ii) The CLEAR control has two functions: first it clears all registers and secondly it removes one input from the input AND gate to the clock control bistable. This causes the clock to be disconnected from the registers, ensuring that once CLEAR has been operated the circuit does not restart until desired.
- (iii) Operation of the HOLD control simply removes the clock in a similar manner to operation of CLEAR but the register contents are held.
- (iv) Operation of the RUN control applies an input to the clock control bistable which allows the clock to be directed through to the registers.
- (v) The clock may be an external pulse generator for continuous operation or the manual step type, with contact bounce suppression, as illustrated.

### 3.2 7-bit Comparator

This compares the 7-bit random input  $R$  with a reference 7-bit number  $F$ , and produces a '1' output pulse when  $R \geq F$ .

The design of such a comparator is a fairly complex exercise in logic design requiring a considerable number of circuit modules. However by using medium scale

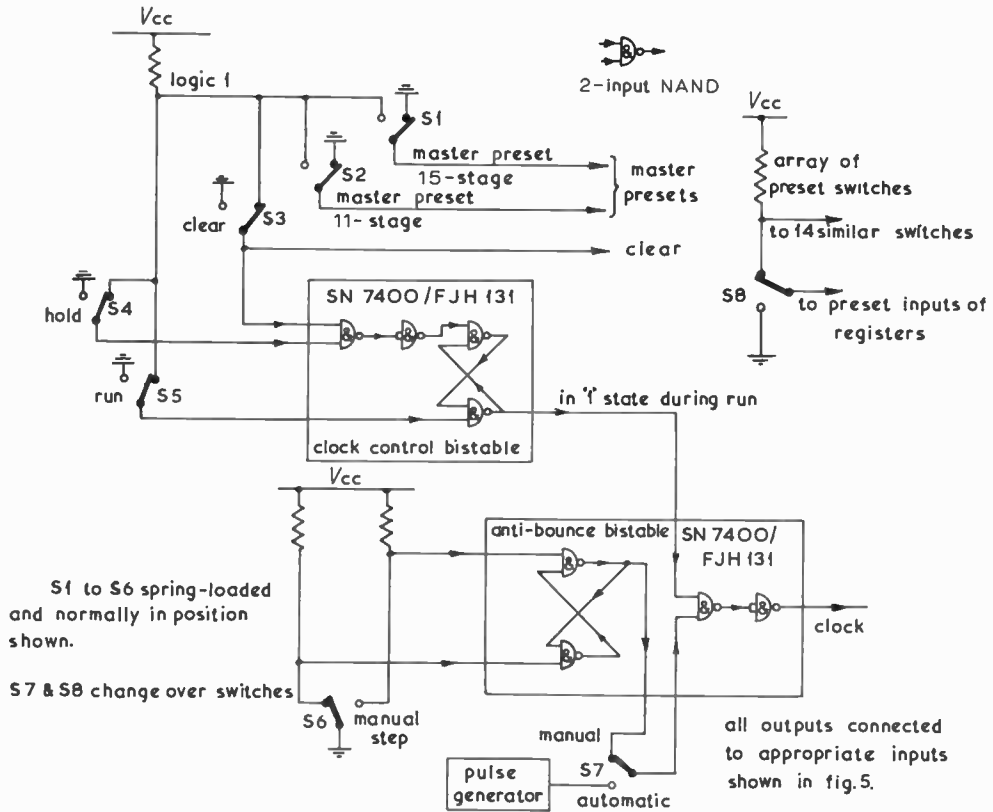


Fig. 6. Control unit of noise generator.

integrated circuits the operation may be implemented using only four packages as illustrated in Fig. 7.

The SN7485 is a package containing a complete 4-bit comparator with facilities for cascading to other similar packages to enable comparators of any length to be made. Therefore two such devices were required for the present application. The resulting combination of two SN7485s produced three outputs for the conditions,  $R = F$ ,  $R > F$  and  $R < F$ , whilst the desired system output occurs when  $R \geq F$ . This is simply achieved by feeding the  $R = F$  and  $R > F$  outputs into a two-input OR. Figure 7 shows the circuit which utilized an SN7400 quad two-input NAND gate connected to give an OR operation. The type of output from the OR gate of Fig. 7

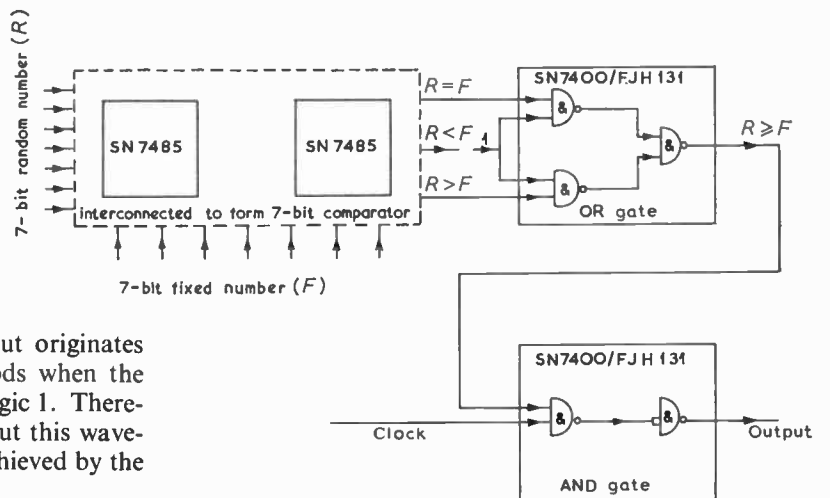
### 3.3 7-bit Reference Number

In its simplest form this consists of switches producing either logic 0 or 1. However more sophisticated arrangements are possible. Linear voltage control of average rate may be achieved by using an analogue to digital converter.

### 4. Tests on the Generator

Detailed statistical tests on generators using similar principles have been reported elsewhere<sup>7, 8</sup> and particularly by Hartley.<sup>9-11</sup> The latter used combined methods of coarse and fine control for varying the output rate and achieved control in steps of (coarse rate)/32. The equipment described here dispensed with the coarse

Fig. 7. 7-bit comparator.



is illustrated in Fig. 3(b). Since this output originates from the registers there are multiple periods when the wave-form at this point stays at logic 0 or logic 1. Therefore in order to produce a pulse train output this wave-form must be gated by the clock. This is achieved by the final AND gate in Fig. 7.

controls and, by using 7-bit numbers, control in steps of 1/128 of the basic rate was possible. It is expected that results for this generator will have properties similar to the combined method although detailed tests have still to be carried out. The results of a 'rate of arrival' test are given in Fig. 8. This is not a complete test for randomness but simply a count of the number of '1' outputs over an extended period of time.

The extraction of the necessary data from experimental records is very demanding and to ease analysis a digital computer program was produced which was an exact digital simulation of the hardware and therefore produced identical output sequences. Details of the flow chart are given in Appendix 2.

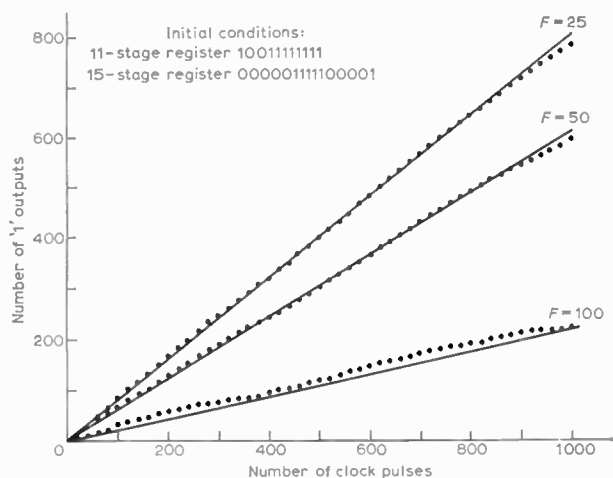


Fig. 8. Arrival test results for a sample length of 20. Full lines—expected values, dots—measured values.

For a rate of arrival test the exact output sequence is not required, it is only necessary to sum the number of '1' outputs over an extended range of input clock pulses. Therefore the program was arranged so that the number of '1' outputs in any required sample length up to any required total of input clock pulse was presented. Figure 8 shows the results for a sample length of 20 up to a total count of 1000 for 'F' values of 25, 50 and 100.

Due to the short sample length of only 20 there are slight deviations from the expected rates for all cases. The results are a realistic simulation of the situation in which the instrument is to be used, since short runs are needed to reduce subject fatigue. Each clock pulse corresponds to a required decision, i.e. detection or no detection. It is hoped to produce more detailed statistical results for short length samples in a subsequent paper.

5. Discussion

This paper has given design details of a random pulse generator with controllable rate which may be simply constructed using integrated circuits. A digital simulation has proved useful for checking the validity of the design. Digital programs of this type are consuming of computer

time and whilst they are useful for confirming the validity of the noise generator it is likely that the hardware simulation of the complete system (Fig. 2) will yield results faster than a digital simulation. This aspect has still to be examined.

Some modifications to the noise generator have been suggested by Hartley<sup>10,11</sup> enabling shorter length registers to be used. However it would appear that the number of outputs is restricted. Eleven and 15-stage registers were used here in order to produce two independent 7-bit numbers. Furthermore the engineering of 11- and 15-stage chain code generators is no longer a problem when modern integrated circuits are used.

6. Acknowledgments

The authors are grateful to Mr. G. Gibson for assisting with the construction of the instruments and Mr. G. J. Blackledge for helpful discussions.

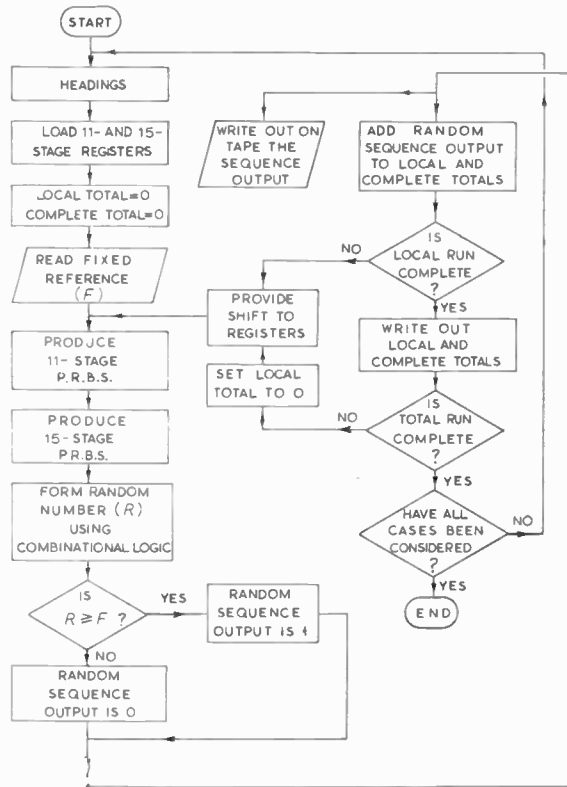
7. References

1. Barr-Hamilton, R. M., Tempest, W. and Bryan, M. E., 'The differential detectability index: a new monaural test for the locus of hearing disorders?', *Sound*, 5, pp. 2-6, February 1971.
2. Korn, G. A., 'Random-Process Simulation and Measurements' (McGraw-Hill, New York, 1966).
3. Davies, W. D. T., 'Generation and properties of maximum-length sequences', *Control*, 10, pp. 302-4, 364-5 and 431-3, June, July and August 1966.
4. Anderson, G. C., Finnie, B. W. and Roberts, G. T., 'Pseudo-random and random test signals', *Hewlett Packard J.*, 19, pp. 2-17, September 1967.
5. Murry, H. F., 'A general approach for generating natural random variables', *I.E.E.E. Trans. on Computers*, C-19, pp. 1210-13, December 1970.
6. Hanby, J. A. and Redman, S. J., 'Random pulse train generator with linear voltage control of average rate', *Rev. Sci. Instrum.*, 42, pp. 657-62, May 1971.
7. Redshaw, S., 'A Repeatable Random Pulse Generator using Chain Codes', M.Sc. (Tech.) Thesis, University of Manchester, 1961.
8. Robinson, P. H., 'Two Types of Random Pulse Generator with Multiple Independent Outputs', M.Sc. (Tech.) Thesis, University of Manchester, 1963.
9. Hartley, M. G., 'Evaluation of performance of random generators employing chaincodes', *Proc. Instn Elect. Engrs*, 116, pp. 27-34, January 1969.
10. Hartley, M. G., 'Development, design and test procedures for random generators using chaincodes', *Proc. Instn Elect. Engrs*, 116, pp. 22-26, January 1969.
11. Hartley, M. G., 'Modelling Techniques for Traffic Studies', Ph.D. Thesis, University of Manchester, 1968.

8. Appendix 1: Alternative connexions from 15-stage and 11-stage generators to combinational logic

$$\begin{aligned}
 &X_{10} \oplus Y_5 \\
 &X_1 \oplus Y_{11} \\
 &X_9 \oplus Y_6 \\
 &X_{11} \oplus Y_4 \\
 &X_3 \oplus Y_{10} \\
 &X_{15} \oplus Y_1 \\
 &X_6 \oplus Y_8
 \end{aligned}$$

9. Appendix 2: Program flowchart for rate of arrival test in noise generator



Manuscript received by the Institution on 26th April 1972. (Paper No. 1473/C148.)

© The Institution of Electronic and Radio Engineers, 1971

# Statistical Stability in Spectrum Analysis

R. E. BOGNER,  
M.E., C.Eng., M.I.E.E.\*

## SUMMARY

Some very simple results which are of use in designing the smoothing system for a digital spectrum analyser, to reduce fluctuations due to the random nature of the envelope of the output of a narrow-band filter are deduced. The 'signal/noise ratio', defined on a mean square basis, of each observation of envelope-squared is unity. The smoothing schemes operate by averaging several observations of envelope-squared, taken at different times or at different frequencies. The discussion shows the relative insensitivity of the result to fine details of the averaging system.

\* Electrical Engineering Department, Imperial College, London, SW7 2BT.

## 1. Introduction

A typical spectrum analyser is based on the system shown in Fig. 1(a). The variables indicated in Fig. 1(a) are:  $u$  = input signal to be analysed,  $v$  = output from narrow band analysing filter,  $x$  = detected version of  $v$ ,  $y$  = output from smoothing filter. In conventional analogue systems the smoothing filter (usually inherent in the dynamics of the indicator) typically has a time constant effectively infinite compared with that of the narrow band filter (at least for r.f. measurements where the values may be, for example, of the order 0.1 s and 0.0002 s respectively). The indicator then has negligible fluctuation about the true mean of the detected envelope,  $x$ . To ensure such luxurious smoothing that  $y$  has negligible fluctuation may require uneconomically long signal records for the input  $u$  in digital processing, and thus it is necessary to be able to predict error statistics.

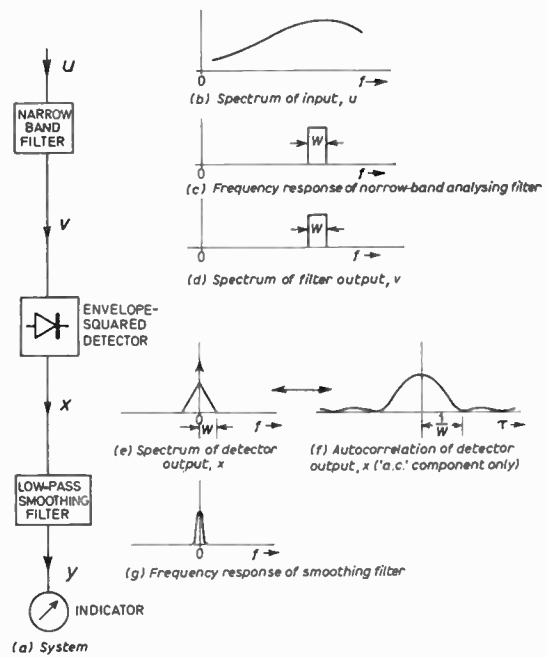


Fig. 1. Basic analyser system.

Previous discussions of some thoroughness<sup>1, 2</sup> appear to have left many engineers without an appreciation of the simplicity with which useful, approximate results may be obtained and used. It is hoped to fill this gap. The results presented have been found useful in proportioning digital systems for spectral analysis, both with fast Fourier transforms and with recursive filters and also correlation analysers.

The error statistics are readily estimated in two stages, for the case where

(i) The input,  $u$ , is real and Gaussian. The latter is frequently very close to the truth, and yields very simple results. Specific non-Gaussian problems are almost invariably of limited applicability and lose intuitive appeal because of the necessity to include higher order moments.

(ii) The detector is a square-law detector, or a squared-envelope detector. This is almost invariably the case in

digital processing since it is convenient to operate on the squared magnitudes of Fourier transform values, or on autocorrelations.

(iii) The band-pass filter has a rectangular pass-band and the input  $u$  has a spectrum which is effectively flat over the pass-band, yielding a rectangular output spectrum (Fig. 1(d)). Sutcliffe<sup>3</sup> derives some related results for an analogue system, showing that reliance on this assumption is not critical.

(iv) The smoothing filter operates by adding with equal weights a number  $M$  of its inputs,  $x$ . Later, this assumption is relaxed.

There are two stages in the consideration:

- (i) description of the statistics of  $x$
- (ii) addition of  $M$  values of  $x$  to form  $y$ .

## 2. Description of the Statistics of $x$

For  $u$  as specified,  $v$  may be described by means of sine and cosine components  $v_R$  and  $v_I$  referred to an arbitrary reference frequency<sup>4</sup> (or 'complex demodulates'<sup>2</sup>). Now  $v_R$  and  $v_I$  are jointly Gaussian and instantaneously independent with zero means,<sup>4</sup> and equal variances,  $\sigma$ . Let the square of the envelope be  $x$ , i.e.

$$x = v_R^2 + v_I^2$$

which is detected by the envelope-squared detector. This is equivalent to the effective base-band component after square-law detection. Then, as shown in the Appendix,  $x$  has the exponential probability density function

$$p(x) = \begin{cases} \frac{1}{2\sigma^2} \exp\left(-\frac{x}{2\sigma^2}\right), & x \geq 0 \\ 0 & x < 0 \end{cases} \quad \dots\dots(1)$$

which yields:

mean  $x$ :

$$\langle x \rangle = \int_0^\infty x p(x) dx = 2\sigma^2 \quad \dots\dots(2)$$

mean square  $x$ :

$$\langle x^2 \rangle = \int_0^\infty x^2 p(x) dx = 8\sigma^4 \quad \dots\dots(3)$$

variance of  $x$  about its mean, or mean square of error  $e$  in estimation of mean of  $x$ :

$$\langle (x - \langle x \rangle)^2 \rangle = 4\sigma^4. \quad \dots\dots(4)$$

A beautifully simple result is evident: if we regard  $\langle x \rangle$ , the mean it is desired to estimate as 'signal' and the error  $e$  as 'noise', then the signal/noise power ratio of each observation of  $x$  is unity (i.e.  $(2\sigma^2)^2/4\sigma^4$ ). This result is independent of the shape of the characteristic of the band-pass filter. We have used so far only assumptions (i) and (ii), concerning the signal statistics and detector law.

Assumption (iii) implies that the spectrum of the band-pass filter output  $v$  is rectangular (Fig. 1(d)). Hence the spectrum after the squared-envelope detector, which is the convolution of the spectrum of  $v$  with itself,<sup>4</sup> has a spike at zero and a triangular baseband component (Fig. 1(e)), of half-width  $W$  Hz. A similar result is obtained for the spectrum of  $x$  for the envelope-squared detector. Then the autocorrelation  $R_{xx}(\tau)$  for the random

component of  $x$  is of the form (Fig. 1(f))

$$R_{xx}(\tau) = \left(\frac{\sin \pi W \tau}{\pi W \tau}\right)^2 \quad \dots\dots(5)$$

whose zeros are spaced at  $1/W$  seconds. This does not necessarily imply that values of  $x$  taken  $W$  seconds apart are independent because  $x$  is not Gaussian, but it does mean that correlation coefficient between  $1/W$  spaced values of  $x$  is zero (ignoring the desired d.c. term).

## 3. Addition of $M$ Values of $x$ to Form $y$

The low-pass filtering or smoothing or averaging can be carried out by summing  $M$  values of  $x$ , (and perhaps normalizing). Let the  $k$ th value of  $x$  be related to the true mean by the  $k$ th error,  $e_k$

$$x_k = \langle x \rangle + e_k.$$

Then the sum is

$$y = \sum_{k=1}^M (\langle x \rangle + e_k) = M\langle x \rangle + \sum_{k=1}^M e_k.$$

If the  $e_k$  are not correlated, i.e. if the  $x_k$  are values taken  $1/W$  Hz apart, then the errors add energywise, and we have, from eqns. (2) and (4):

$$\langle y \rangle = M\langle x \rangle = 2M\sigma^2$$

$$\langle (y - \langle y \rangle)^2 \rangle = M\langle e_k^2 \rangle = 4M\sigma^4.$$

Then the 'signal/noise ratio' of the observation  $y$  is  $M$ , thus:

$$\frac{\langle y \rangle^2}{\langle (y - \langle y \rangle)^2 \rangle} = (2M\sigma^2)^2/4M\sigma^4 = M. \quad \dots\dots(6)$$

This approach to smoothing is practical, and advantageous over spectral smoothing of Fourier transformed values (described later) in the case where the spectrum is to be estimated at a few points only, or where long data sequences would require excessive storage.

## 4. Applications of Smoothing Result: Spectral Interpretation

A direct application of eqn. (6) by summing  $M$  values of  $x$  is practical; it may be carried out continually in a digital filter whose impulse response is as shown in Fig. 2(a).

$$h_k = \begin{cases} 1, & k = 0, M, 2M, \dots, (M-1)N \\ 0 & \text{otherwise} \end{cases}$$

so that  $y_k$  is obtained from the convolution

$$y_k = \sum_{r=0}^M h_r x_{k-r} = x_k + 0 + \dots + 0 + x_{k-N} + 0 + \dots + x_{k-2N} + \dots + x_{k-(M-1)N}. \quad \dots\dots(7)$$

The value of  $N$  could be chosen to satisfy the uncorrelatedness criterion noted below equation (5),

$$NT = 1/W$$

where  $T$  is the sampling interval. It will soon be evident that this is not strictly necessary. In fact the discussion of smoothing in terms of uncorrelated sample additions is simply one route to the result, which will be shown to be much more widely applicable, albeit with approximation. To avoid the need to take notice in programming of the discrete block length,  $N$ , and to have available a con-

tinually updated estimate of  $y$ , we consider the case where  $N = 1$  (Fig. 2(b)), i.e.

$$h_k = \begin{cases} 1, & k = 0, 1, 2, \dots, (M-1)N \\ 0 & \text{otherwise} \end{cases}$$

which is a sampled data approximation to a finite-duration integrator.

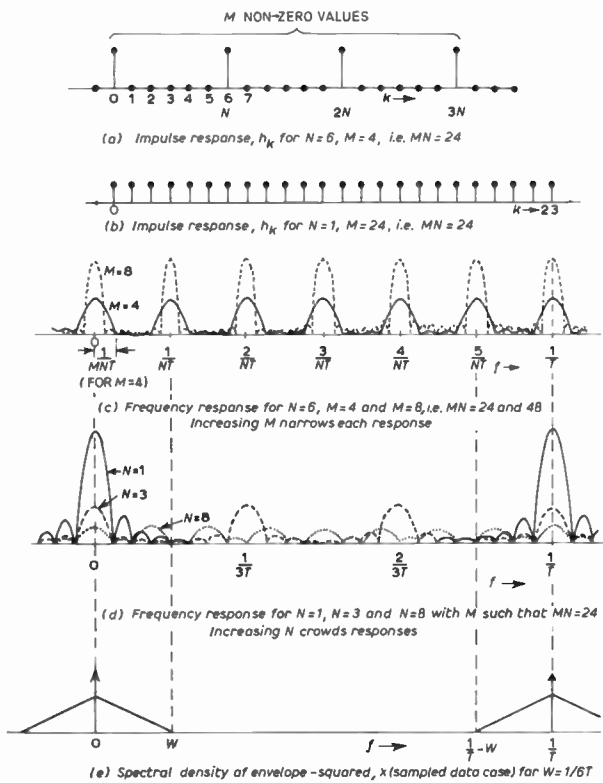


Fig. 2. Spectral descriptions in time-smoothing.

The frequency characteristics of these filters are found by writing  $H(z)$  with  $\exp(j2\pi fT)$  substituted for  $z$ :

$$\begin{aligned}
 H(f) &= 1 + \exp(-j2\pi fNT) + \exp(-j2\pi f2NT) + \\
 &\quad + \exp(-j2\pi f3NT) + \dots + \\
 &\quad + \exp[-j2\pi fN(M-1)T] \\
 &= \frac{1 - \exp(-j2\pi fMNT)}{1 - \exp(-j2\pi fNT)} \\
 &= \exp[-j\pi fNT(M-1)] \cdot \frac{\sin j\pi fMNT}{\sin j\pi fNT} \quad \dots\dots(8)
 \end{aligned}$$

It is helpful to note that the magnitude of  $H(z)$  as given by the ratio term of eqn. (8) approximates a sinc shape when  $fNT$  is close to an integer. Frequency characteristics are shown in Figs. 2(c) and 2(d).

Three important features are evident:

- (a) The response is 'periodic' in frequency, with period  $1/NT$  Hz, i.e. dependent on the sample spacing.
- (b) The half-width of the main responses, and also the spacing between zeros is  $1/MNT$  Hz, i.e. dependent on the overall duration of the response. The number of zeros in each period is  $M-1$ .
- (c) The shape of each main response is substantially independent of the presence of other responses

provided  $M$  is larger than about 5 as this ensures that the sidelobes of the repeated responses do not interfere significantly.

The spectral relations between the squared-envelope  $x$  and the smoothing filter  $h$  are shown by comparing Figs. 2(c) and 2(d) with 2(e). The value for  $N$  of 6, used in Fig. 2(c), has been chosen in accordance with the uncorrelatedness condition  $NT = 1/W$  and  $W = 1/6T$ . We see that the filter lobe at  $1/NT$  occurs just at the edge of the spectrum of  $x$ , and thus contributes little to the output  $y$ . We would thus expect that decreasing the value of  $N$  (Fig. 2(d)) which merely puts the non-zero-frequency main lobes further away would cause little change in the output signal/noise ratio, provided the overall duration of the response  $(M-1)N$  is maintained. (Note that more than the theoretically-needed number of contributions to achieve this result are used.)

On the other hand, increasing  $N$  beyond that required for uncorrelatedness for a constant overall duration would place more main lobes in the band 0 to  $W$  and hence increase the output noise without increasing the signal contributed at zero frequency.

Increasing the overall 'duration'  $(M-1)N$  (Fig. 2(c)) decreases the width of each main lobe, and is the way we can improve the signal/noise ratio if  $N$  is not increased as well. This is the procedure which leads to result given in eqn. (6).

Other smoothing filters are possible. The essential 'signal/noise' behaviour is predictable from the foregoing discussion, in terms of spectral descriptions and effective bandwidths, and the simplicity of the results is especially attractive. From fundamental  $\Delta T, \Delta f$  considerations it should not be possible to do significantly better in a mean-square sense than the constant-weighting filters discussed although it may be that some weightings give a more subjectively acceptable smoothing when rare fluctuations occur.

In slightly different contexts, other smoothing filter windows have been extensively discussed<sup>1</sup>; the application has usually been to spectrum displays, and the averaging has often been carried out over frequency domain samples rather than over time domain samples. The ideas are illustrated in the next section.

### 5. Spectral Smoothing

The discussion on time smoothing can be related to the established procedure of frequency smoothing for spectral analysis via discrete and fast Fourier transforms.

It should be noted that each frequency-domain value  $U_k$  of a Fourier transform,

$$U_k = \sum_{n=0}^{N-1} u_n \exp\left(-j\frac{2\pi nk}{N}\right) \quad \dots\dots(9)$$

is equivalent to the output  $v_n$  of a digital filter, evaluated at  $n=0$ , when the input is  $u_n$  and the impulse response  $h_{n,k}$  is

$$h_{n,k} = \begin{cases} \exp\left(j\frac{2\pi nk}{N}\right), & n = -(N-1), \dots, 0 \\ 0 & \text{elsewhere} \end{cases} \quad \dots\dots(10)$$

where  $k$  is an integer.

It may be noted that although this impulse response is non-causal and hence non-realizable it is realizable if an appropriate delay is allowed. The output  $v_{n,k}$  for  $n = 0$  by convolution is then written:

$$v_{0,k} = \sum_{r=-\infty}^{\infty} u_r h_{0-r} = \sum_{r=-(N-1)}^0 u_r \exp\left(-j \frac{2\pi r k}{N}\right) \dots\dots(11)$$

Comparison with eqn. (9) proves the equivalence.

The frequency response of the filter described by eqn. (10) is readily found to be of the form

$$|H(f)| = \left| \frac{\sin N\pi(f - k/NT)T}{\sin \pi(f - k/NT)T} \right|$$

For  $f - k/NT$  small compared with  $1/T$ , this behaves like a sinc function.

The use of a discrete Fourier transform is illustrated in Fig. 3(a). The lower right shows the time function  $u(t)$ , of which a record of  $M \cdot N$  samples is available. Consider one frequency band filter as specified in eqn. (11). Its output envelope as a function of time would be one of the many functions  $x_0(t), x_1(t), x_2(t)$  etc. This is the function whose square we discussed smoothing by averaging over  $M$  values, spaced  $N$  apart. An independent value is available every  $N$  input samples, and these values are shown by the vertical lines in the diagram. Having on the way calculated  $NM$  unsmoothed values, one ends up with  $N$  smoothed values.

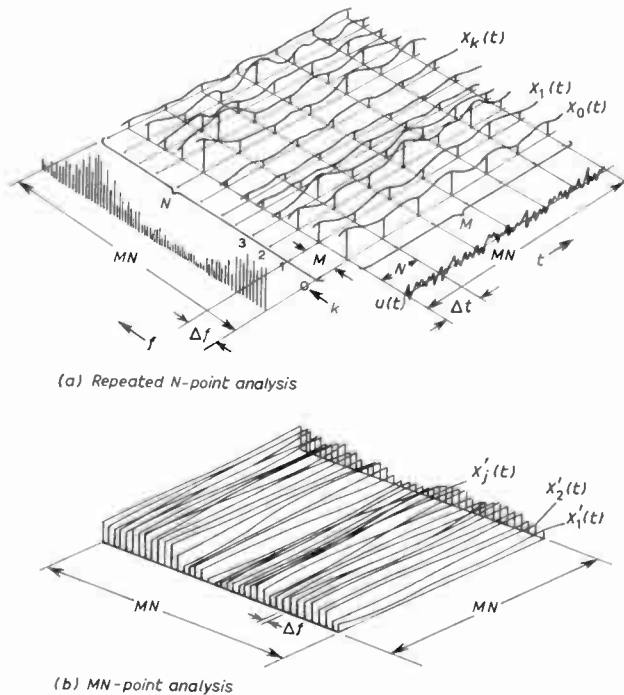


Fig. 3. Equivalence of time and frequency resolutions.

Now, fast Fourier transforms provide the most spectacular advantages in efficiency for large numbers of points or samples. The number of operations for  $N$  points is approximately proportional to  $N \cdot \log_2 N$  so that the number required for finding all the  $M$  values for

each  $x_k(t), k = 1 \dots N$  is  $MN \cdot \log_2 N$ . Then the time smoothing has to be done for each  $x_k(t)$ . A convenient procedure which is now widely used, and is economic if one wants the whole spectrum, is to transform all  $MN$  values, using  $MN \cdot \log_2 MN$ , a slight penalty having been incurred. The smoothing is then conveniently carried out on the  $MN$  frequency values shown on the lower left of Fig. 3(a). These values correspond to the envelopes-squared  $x'_j(t)$  of  $MN$  narrow-band filters and each has slower time-variation than the  $x_k(t)$ , as shown in Fig. 3(b). Each  $x'_j(t)$  is considered to contribute one independent output for  $MN$  time-samples of input.

The assumption of independence between  $x'_j(t)$  is not strictly true in general. It would be true in one case of special interest: when the original  $u_n$  are independent, corresponding *inter alia* to their having a flat spectrum. Then any linear combinations of them such as the Fourier transform eqn. (9) or convolution eqn. (11) yield independent values. When the spectrum of  $u_n$  is fairly smooth, then its behaviour close to a given frequency is similar to that of the constant spectrum. Thus one can operate as in the case of time-smoothing.

The smoothing is carried out in the frequency domain by combining several adjacent values of the  $MN$  narrow-band filter energies  $x'_j(t)$ . A direct parallel to the time-smoothing argument would involve adding together the  $M$  values contributing to the band  $\Delta f$  (bottom left, Fig. 3(a)). Usually, the contributions to each output are weighted, yielding an effective frequency response of the spectrum analysing function more similar to the behaviour of conventional analogue filters, giving less leakage from remote components and smoother behaviour for sharp features. The equivalent 'bandwidths' of smoothing filters of shapes other than rectangular (i.e. equal weights for each of the  $M$  contributions) are readily found by summing the squares of the weights. The results are given in Fig. 4 for a number of popular windows, for the case where  $M$  is large. The values given were in fact calculated by integration for the continuous waveform case. They may be interpreted in either of two equivalent ways:

- (a) As the output signal/noise ratio (mean square) referred to that of an equal-weight system, including  $M$  contributions.
- (b) As the number of equal contributions which would give the same signal/noise ratio—i.e. the equivalent band-width (in samples).

(The examples given are based on those given by Blackman and Tukey<sup>1</sup>, but calculated differently.)

### 6. Conclusions

Attention has been drawn to the simple result that the envelope-squared of the Gaussian output of the narrow-band filter is equivalent to a signal with unity signal/noise ratio, where the 'signal' is the true mean and the 'noise' refers to the fluctuation about the mean. Smoothing of this envelope-squared may be accomplished by adding together values spaced sufficiently far apart to be uncorrelated, and the improvement in the signal/noise ratio is directly proportional to the number of values added. If additional values are added which are more

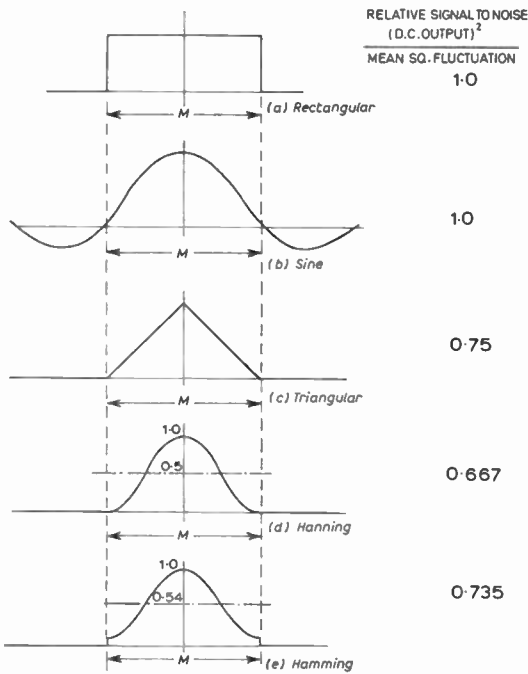


Fig. 4. Performance of some windows.

closely spaced than needed for uncorrelatedness, then no significant improvement nor degradation should be expected if the total number of uncorrelated values is not changed. This latter result is approximate, and is deduced from a spectral description of the smoothing filtering.

It has been shown how the same philosophy of smoothing, and the results, are applicable to the practice of smoothing in the frequency domain of values of the squares of Fourier components.

7. Acknowledgments

The work was carried out in the context of simulation studies of communication systems, which were supported by Government Communications Headquarters. The author is grateful to the (anonymous) referee whose comments indicated several points needing clarification and who suggested the simple treatment given in the Appendix; also to Claude Vouga and Sinclair Budd whose simulations provided a vehicle for developing the ideas discussed here.

8. References

- Blackman, R. B. and TUKEY, J. W., 'The measurement of power spectra from the point of view of communication engineering', *Bell Syst. Tech. J.*, 37, p. 185, January 1958, and 37, p. 485, March 1958.
- Bingham, C. et al., 'Modern techniques of power spectrum estimation', *I.E.E.E. Trans. on Audio and Electroacoustics*, AU-15, No. 2, p. 56, June 1967.

- Sutcliffe, H., 'Relative merits of quadratic and linear detectors in the direct measurement of noise spectra', *The Radio and Electronic Engineer*, 42, p. 65, February 1972.
- Rice, S. O., 'Mathematical analysis of random noise', in 'Selected Papers on Noise and Stochastic Processes', N. Wax (Ed.) (Dover, New York, 1954).

9. Appendix

It can be shown that the probability density function  $p_x(x)$  of  $x$ , the squared envelope, is exponential. Starting with the cosine and sine components  $v_R$  and  $v_I$  of the input,  $v$  (Fig. 1(a)), and assuming that these are jointly and independently Gaussian,<sup>4</sup>

$$p(v_R) = \frac{1}{\sigma\sqrt{2\pi}} \exp(-v_R^2/2\sigma^2)$$

and

$$p(v_I) = \frac{1}{\sigma\sqrt{2\pi}} \exp\left(-\frac{v_I^2}{2\sigma^2}\right).$$

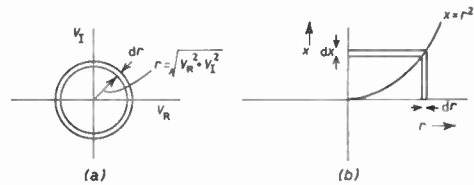


Fig. 5. Transformation of probability densities.

We first find the probability density  $p_r(r)$  where  $r = \sqrt{(v_R^2 + v_I^2)}$ , thus: the probability mass over the annulus of radius  $r$ , Fig. 5(a), is:

$$p_r(r)2\pi r dr = \frac{1}{\sigma^2 2\pi} \exp\left(-\frac{r^2}{2\sigma^2}\right) 2\pi r dr, r > 0$$

Therefore,

$$p_r(r) = \frac{r}{\sigma^2} \exp\left(-\frac{r^2}{2\sigma^2}\right),$$

the familiar Rayleigh density function. Then the density of  $x = r^2$ ,  $r > 0$ , is found by equating the probabilities (Fig. 5(b)):

$$\text{prob}(x \text{ lies in } dx \text{ at } x) = \text{prob}(r \text{ lies in } dr \text{ at } r),$$

$$\text{i.e. } p_x(x) dx = p_r(r) dr$$

$$p_x(x) = \frac{r}{\sigma^2} \exp\left(-\frac{r^2}{2\sigma^2}\right) \frac{dr}{dx}$$

$$= \frac{1}{2\sigma^2} \exp(-x/2\sigma^2).$$

Manuscript first received by the Institution on 5th January 1972 and in revised form on 3rd July 1972. (Paper No. 1474/IC67.)

© The Institution of Electronic and Radio Engineers, 1972

# Cascade Synthesis of Driving Point Functions using Non-uniform RC Transmission Lines

**Professor B. B. BHATTACHARYYA,**  
B.Tech., M.Tech., Ph.D.\*

and

**Professor M. N. S. SWAMY,**  
B.Sc.(Hons.), D.I.I.Sc., M.Sc., Ph.D.\*

## SUMMARY

Necessary and sufficient conditions, as well as a synthesis procedure, for realizing a class of driving point functions as a cascade of non-uniform RC transmission lines, are presented. By using known transformations, the results may also be applied to other types of lines, such as lossless lines.

\* Department of Electrical Engineering, Sir George Williams University, Montreal 107, Canada

## 1. Introduction

A number of articles have been written<sup>1-6</sup> on the synthesis of driving point functions using uniform RC transmission lines (URC) or non-uniform RC transmission lines (NURC). It has also been pointed out that it would be useful, from the point of view of fabrication, to have the lines in cascade in any synthesis procedure.<sup>7</sup> However, excepting in the case of URC or symmetric non-uniform lines,<sup>1, 6</sup> no such synthesis procedure employing a cascade of NURCs as yet exists. It is to be noted that both URC and symmetrical NURCs have symmetrical  $[Z]$  matrices, namely, where  $z_{11} = z_{22}$ .

The purpose of this contribution is to present a simple synthesis procedure for driving point functions using a cascade of NURCs. The  $[Z]$  matrix of the NURC may be asymmetrical, that is,  $z_{11}$  in general need not equal  $z_{22}$ .

## 2. The Method

A non-uniform RC line ( $\mathcal{L}$ ) is one characterized by the following distributions for its resistance per unit length  $r(x)$  and capacitance per unit length  $c(x)$ , respectively, where  $x$  is the distance from the input end:

$$\begin{aligned} r(x) &= r_0 f(x) \\ c(x) &= c_0 g(x) \end{aligned} \quad (0 \leq x \leq l) \quad \dots\dots(1)$$

This non-uniform line will be symbolized by the schematic of Fig. 1. This will be referred to as the configuration (a) of the line and is denoted by  $\mathcal{L}_a$ . By switching the terminals we get two more configurations  $\mathcal{L}_b$  and  $\mathcal{L}_c$ , as shown in Fig. 1. The matrix parameters of  $\mathcal{L}_a$ ,  $\mathcal{L}_b$  and  $\mathcal{L}_c$  are interrelated, and are consistent with those given elsewhere for a general 3-terminal network.<sup>8</sup>

It is obvious that a cascade connexion using  $\mathcal{L}_a$  is the only useful one from a practical point of view.

The matrix parameters of the NURC in configuration  $\mathcal{L}_a$  may be determined from either the solutions or directly.<sup>9-11</sup> Let us assume that the chain matrix parameters of the NURC be of the form

$$[a] = \begin{bmatrix} A(s) & B(s) \\ C(s) & D(s) \end{bmatrix} \quad \dots\dots(2)$$

We can now easily put the various one-port impedances available from  $\mathcal{L}_a$  in the following form:

$$1/y_{11} = B/D = Rp_1(s) \quad \dots\dots(3a)$$

$$1/y_{22} = B/A = Rp_2(s) \quad \dots\dots(3b)$$

$$Z_{11} = A/C = Rq_1(s) \quad \dots\dots(3c)$$

$$Z_{22} = D/C = Rq_2(s) \quad \dots\dots(3d)$$

where

$$R = r_0 l. \quad \dots\dots(3e)$$

Let us now define the variable  $u(s)$  as,

$$u(s) = p_1(s)/q_1(s). \quad \dots\dots(3f)$$

It is immediately seen that  $u(s)$  is also equal to  $p_2(s)/q_2(s)$ .

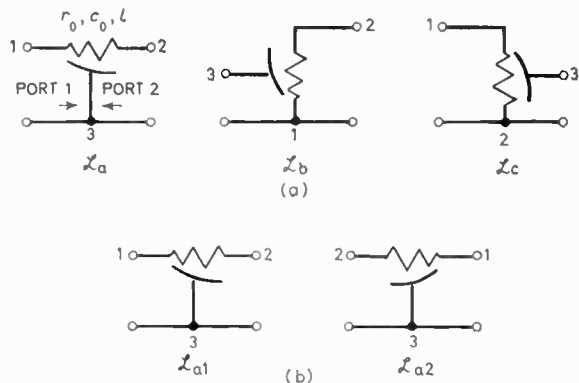


Fig. 1. (a) The three different configurations, namely  $\mathcal{L}_a$ ,  $\mathcal{L}_b$  and  $\mathcal{L}_c$ , of a NURC with distributions  $r = r_0 f(x)$ ,  $c = c_0 g(x)$ , ( $0 \leq x \leq l$ ).  
(b) The two subdivisions  $\mathcal{L}_{a1}$  and  $\mathcal{L}_{a2}$  of the line  $\mathcal{L}_a$ .

For a cascade of symmetric lines, ports 1 and 2 of  $\mathcal{L}_a$  are indistinguishable. However, for an asymmetric line, the impedance looking into port 1 with port 2 terminated in a load is different from that at port 2 with the same termination at port 1. To distinguish these two situations, the configuration  $\mathcal{L}_a$  is subdivided into  $\mathcal{L}_{a1}$  and  $\mathcal{L}_{a2}$  as shown in Fig. 1(b). We shall now establish the following theorem which will directly lead us to the cascade synthesis procedure.

**THEOREM:** The necessary and sufficient condition that a function  $Z(s)$  be realizable as a driving point function of a cascade of NURCs, of constant  $(r_0 c_0 l^2)$  product, where the structures  $\mathcal{L}_{a1}$  and  $\mathcal{L}_{a2}$  alternate and where the end structure may be open or short circuited, is that it be expressible in the form

$$Z(s) = p(s) \{ \text{RC-impedance function in } u(s) \}$$

where

$$p(s) = p_1(s) \text{ or } p_2(s), \text{ and } u = p_1/q_1 = p_2/q_2.$$

**NECESSITY:** To prove the necessary part, let us assume that the given structure consists of  $n$ -sections, with  $\mathcal{L}_{a1}$  and  $\mathcal{L}_{a2}$  alternating each other. Let us assume that the different sections are numbered as shown in Fig. 2, where the section 1 may be open or short-circuited. Then the impedance  $Z_{i+1}(s)$  looking into section  $(i+1)$  may be expressed in terms of  $Z_i$  as

$$Z_{i+1}(s) = \frac{A_{i+1}(s)Z_i(s) + B_{i+1}(s)}{C_{i+1}(s)Z_i(s) + D_{i+1}(s)} \quad \dots\dots(4)$$

Assuming first that the  $i$ th section is an  $\mathcal{L}_{a1}$ , we may use (3) to rewrite (4) in the form

$$\bar{Z}_{i+1}(u) = R_{i+1} \frac{\bar{Z}_i(u) + R_{i+1}}{u\bar{Z}_i(u) + R_{i+1}} \quad \dots\dots(5)$$

where

$$\bar{Z}_i = Z_i/p_2 \text{ and } \bar{Z}_{i+1} = Z_{i+1}/p_1. \quad \dots\dots(6a)$$

Similarly, if the  $i$ th section is an  $\mathcal{L}_{a2}$  we may rewrite (4) in the form (5), where now

$$\bar{Z}_i = Z_i/p_1 \text{ and } \bar{Z}_{i+1} = Z_{i+1}/p_2. \quad \dots\dots(6b)$$

If we now assume that  $\bar{Z}_i(u)$  is an RC-function in  $u$ , then it may be shown that  $\bar{Z}_{i+1}(u)$  is also an RC-function.

Thus, it is seen that if  $Z_i(s)$  is of the form

$$Z_i(s) = p(s) \{ \text{RC-impedance function in } u \} \quad (7a)$$

where

$$p(s) = p_1(s) \text{ or } p_2(s) \quad \dots\dots(7b)$$

then  $Z_{i+1}(s)$  is also of the same form as (7). It may also be verified that for  $i = 1$ , whether that section be an  $\mathcal{L}_{a1}$  or  $\mathcal{L}_{a2}$  and whether it be open or short circuited, the impedance  $Z_1(s)$  is of the form as (7). Hence, by induction the necessity of the theorem follows.

**SUFFICIENCY:** It is known that if we are given an impedance  $Z(s)$  and we extract a two-port with a chain matrix  $[A, B, C, D]$ , then the remaining impedance  $Z_L(s)$  is of the form

$$Z_L(s) = \frac{DZ - B}{A - CZ} \quad \dots\dots(8)$$

Using (8) it may be shown that if we are given an impedance of the form

$$Z(s) = p(s) \{ \text{RC-impedance function in } u, \text{ say } \bar{Z}(u) \} \quad (9a)$$

where

$$p(s) = p_1(s) \text{ or } p_2(s) \quad \dots\dots(9b)$$

we may extract a section  $\mathcal{L}_{a1}$  or  $\mathcal{L}_{a2}$  depending on whether  $p(s) = p_1(s)$  or  $p_2(s)$  respectively. The remaining impedance  $Z_L(s)$  is of the form

$$Z_L(s) = Rq \left[ \frac{Z(s)/p - R}{R - uZ(s)/p} \right] \quad \dots\dots(10)$$

where  $q = p_2$  if  $p = p_1$  while  $q = p_1$  if  $p = p_2$ . Choosing  $(r_0 l) = R$  for this section to be

$$R = \bar{Z}(1) \quad \dots\dots(11a)$$

we may rewrite (10) in the form

$$\frac{Z_L}{q} = \bar{Z}_L(u) = R \frac{\bar{Z}(u) - \bar{Z}(1)}{\bar{Z}(1) - u\bar{Z}(u)} \quad \dots\dots(11b)$$

It can be shown that if  $\bar{Z}(u)$  is an RC-impedance function in  $u$ , so also is  $\bar{Z}_L(u)$  given by (11b).<sup>12</sup> Further,  $Z_L(u)$  is of a lower order of complexity than  $\bar{Z}(u)$ , since  $(u-1)$  is a common factor between the numerator and denominator, and hence can be cancelled out.

We will now propose the following cascade synthesis procedure, and thus establish the sufficiency also.

(i) Given an impedance

$$Z(s) = p(s) \{ \text{RC-impedance function in } u, \text{ say } \bar{Z}_1(u) \} \quad \dots\dots(12a)$$

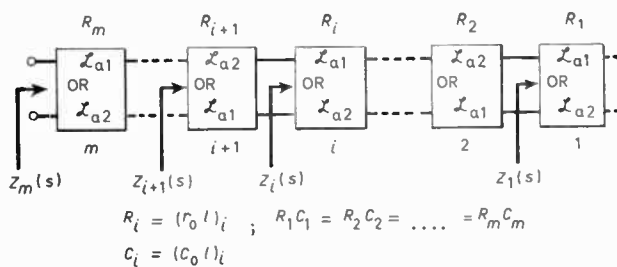


Fig. 2. Cascade structure used in the realization of  $Z(s)$  given by the Theorem.

where

$$p(s) = p_1(s) \text{ or } p_2(s), \quad \dots\dots(12b)$$

obtain the normalized impedance

$$\bar{Z}_1(u) = Z/p. \quad \dots\dots(13)$$

(ii) Depending on whether  $p = p_1$  or  $p_2$ , extract an NURC section  $\mathcal{L}_{a1}$  or  $\mathcal{L}_{a2}$  respectively, such that its  $R_1$  parameter, namely

$$(r_0 l)_1 = R_1 = \bar{Z}_1(1). \quad \dots\dots(14)$$

The other parameter of the NURC, namely  $C_1 = (c_0 l)_1$  may be obtained from the fact that the RC-products ( $r_0 c_0 l^2$ ) of all the sections in the cascade must be the same.

(iii) Obtain the remaining impedance

$$\bar{Z}_2(u) = \bar{Z}_1(1) \frac{\bar{Z}_1(u) - \bar{Z}_1(1)}{\bar{Z}_1(1) - u\bar{Z}_1(u)} \quad \dots\dots(15)$$

which is assured to be an RC-impedance function, and of a lower order of complexity than  $\bar{Z}_1(u)$ , after cancellation of the common factor  $(u - 1)$  between the numerator and denominator of  $\bar{Z}_2(u)$ . It is noted that  $\bar{Z}_2(u)$  is related to its corresponding unnormalized impedance by

$$Z_2(s) = q(s) \{ \text{an RC-impedance function in } u, \text{ namely } \bar{Z}_2(u) \} \quad \dots\dots(16)$$

where  $q = p_2$  or  $p_1$  depending on whether  $p = p_1$  or  $p_2$  respectively in (12). Thus the impedance  $Z_2(s)$  given by (15) is of the same form as  $Z(s)$  given by (12), and hence one cycle in the synthesis is completed.

(iv) Repeat the process till the remainder is of the form  $p(s)[R_n/u]$  or  $p(s)[R_n]$ ; which may be realized by an open or short circuited section of  $\mathcal{L}_{a1}$  or  $\mathcal{L}_{a2}$ . This completes the realization of the given  $Z(s)$ .

It should be observed that in the synthesis procedure given above, the sections  $\mathcal{L}_{a1}$  and  $\mathcal{L}_{a2}$  are extracted alternately, the first section removed being an  $\mathcal{L}_{a1}$  or  $\mathcal{L}_{a2}$  depending on whether  $p = p_1$  or  $p_2$  in the given impedance (12a).

### 3. Conclusions

Thus we have given a necessary and sufficient condition, as well as a simple synthesis procedure, for realizing a class of driving point functions as a cascade of tapered NURCs. It should be mentioned that for a symmetric NURC, the sections  $\mathcal{L}_{a1}$  and  $\mathcal{L}_{a2}$  are the same, and hence cascade synthesis using symmetric NURCs (and hence using URCs) is a special case of the procedure developed here. Further, it is noted that although our

development has been restricted to the consideration of RC-lines, it is equally applicable to driving point function synthesis using LC, RCG and distortionless RLCG lines, in view of the results given elsewhere.<sup>9</sup>

### 4. Acknowledgment

This work was supported by the National Research Council of Canada, Grants No. A-7740 and A-7739.

### 5. References

1. Wyndrum, Jun., R. W., 'The Exact Synthesis of Distributed RC Networks', New York University Technical Report 400-76, Department of Electrical Engineering, May 1963.
2. Wyndrum, Jun., R. W., 'The realization of monomorphic thin-film distributed RC networks', *I.E.E.E. Int. Conv. Rec.*, 13, Pt 10, pp. 90-5, 1965.
3. O'Shea, R. P., 'Synthesis using distributed RC networks', *ibid.*, Pt. 7, pp. 18-29.
4. Giguere, J. C., Swamy, M. N. S. and Bhattacharyya, B. B., 'Driving point function synthesis using tapered RC lines and their duals', *I.E.E.E. Trans. on Circuit Theory*, CT-16, pp. 93-4, February 1969.
5. Lee, S. C., 'Synthesis of tapered distributed RCG networks', *I.E.E.E. Trans. on Circuit Theory*, CT-16, pp. 57-67, February 1969.
6. Giguere, J. C., Swamy, M. N. S. and Bhattacharyya, B. B., 'Driving point function synthesis using nonuniform lines', *Proc. Instn. Elect. Engrs.*, 116, No. 1, pp. 65-70, January 1969.
7. Ghauri, M. S. and Kelly, J. J., 'Introduction to Distributed-Parameter Networks: with Applications to Integrated Circuits', (Holt, Rinehart and Winston, London, 1968).
8. Swamy, M. N. S., 'On the matrix parameters of a 3-terminal network', *Proc. Inst. Elect. Electronics Engrs.*, 54, pp. 1081-2, August 1966.
9. Bhattacharyya, B. B., 'Some General Properties and Solutions of Non-uniform Transmission Lines', Ph.D. Thesis, Nova Scotia Technical College, Halifax, Canada, 1968.
10. Protonotarios, E. N. and Wing, O., 'Delay and risetime of arbitrarily tapered RC-transmission lines', *I.E.E.E. Int. Conv. Rec.*, 13, Part 7, pp. 1-6, 1965.
11. Swamy, M. N. S., 'Matrix parameters of an arbitrarily tapered RC line', *Proc. Mid-American Electronics Conf.*, 1965, pp. 79-82.
12. Stein, J. J., Mulligan, Jr., J. H. and Shamis, S. S., 'Realization of Transfer Functions using Uniform RC-Distributed Networks with Common Ground Connections', *Proc. Symp. on Generalized Networks*, Brooklyn Polytech. Institute, 1966, pp. 149-172.

Manuscript received by the Institution on 10th May 1972. (Short Contribution No. 158/CCI49)